Lithos 116 (2010) 209–229

Contents lists available at ScienceDirect

Lithos

journal homepage: www.elsevier.com/locate/lithos

Subduction styles in the Precambrian: Insight from numerical experiments

E. Sizova [a,*], T. Gerya [a,b], M. Brown [c], L.L. Perchuk [d,e]

[a] Institute of Geophysics, ETH-Zurich, Sonnegstrasse, 5, 8092 Zurich, Switzerland
[b] Geology Department, Moscow State University, 119199 Moscow, Russia
[c] Department of Geology, University of Maryland, College Park, MD, 20742, USA
[d] Department of Petrology, Moscow State University, 119199 Moscow, Russia
[e] Faculty of Science, University of Johannesburg, South Africa

ARTICLE INFO

Article history:
Received 23 January 2009
Accepted 27 May 2009
Available online 18 June 2009

Keywords:
Precambrian
Tectonics
Subduction
Numerical modeling
Melt-related weakening

ABSTRACT

Plate tectonics is a self-organizing global system driven by the negative buoyancy of the thermal boundary layer resulting in subduction. Although the signature of plate tectonics is recognized with some confidence in the Phanerozoic geological record of the continents, evidence for plate tectonics becomes less certain further back in time. To improve our understanding of plate tectonics on the Earth in the Precambrian we have to combine knowledge derived from the geological record with results from well-constrained numerical modeling.

In a series of experiments using a 2D petrological–thermomechanical numerical model of oceanic subduction we have systematically investigated the dependence of tectono-metamorphic and magmatic regimes at an active plate margin on upper-mantle temperature, crustal radiogenic heat production, degree of lithospheric weakening and other parameters. We have identified a first-order transition from a "no-subduction" tectonic regime through a "pre-subduction" tectonic regime to the modern style of subduction. The first transition is gradual and occurs at upper-mantle temperatures between 250 and 200 K above the present-day values, whereas the second transition is more abrupt and occurs at 175–160 K. The link between geological observations and model results suggests that the transition to the modern plate tectonic regime might have occurred during the Mesoarchean–Neoarchean time (ca. 3.2–2.5 Ga). In the case of the "pre-subduction" tectonic regime (upper-mantle temperature 175–250 K above the present) the plates are weakened by intense percolation of melts derived from the underlying hot melt-bearing sub-lithospheric mantle. In such cases, convergence does not produce self-sustaining one-sided subduction, but rather results in shallow underthrusting of the oceanic plate under the continental plate. Further increase in the upper-mantle temperature (>250 K above the present) causes a transition to a "no-subduction" regime where horizontal movements of small deformable plate fragments are accommodated by internal strain and even shallow underthrusts do not form under the imposed convergence. Thus, based on the results of the numerical modeling, we suggest that the crucial parameter controlling the tectonic regime is the degree of lithospheric weakening induced by emplacement of sub-lithospheric melts into the lithosphere. A lower melt flux at upper-mantle temperatures <175–160 K results in a lesser degree of melt-related weakening leading to stronger plates, which stabilizes modern style subduction even at high mantle temperatures.

1. Introduction

Two fundamental questions about subduction styles in the Precambrian have been the subject of debate during the past decade (e.g. Davies, 1992; Hamilton, 1998; de Wit, 1998; Griffin et al., 2003; Davies, 2006; Brown, 2006, 2007; Stern, 2007; O'Neil et al., 2007a,b; van Hunen and van den Berg, 2008) first, what was the reason that Earth developed a plate tectonics regime; and, second, what was the timing of the transition to the plate tectonics regime on Earth? The main arguments about the timing of initiation of plate tectonics have been based on the interpretation of geological, petrological and geochemical observations (Benn et al., 2005; Condie and Pease, 2008). It is only recently that parameterized numerical modeling experiments have been used to investigate both of these questions (e.g. Davies, 2006; O'Neil et al., 2007a,b; Sleep, 2007; van Hunen and van den Berg, 2008).

The interpretation of geological observations has not achieved a consensus about the style of the tectonic regime in the Precambrian. On the one hand, there is a variety of evidence for Archean, particularly Mesoarchean-to-Neoarchean, plate tectonics and subduction settings (e.g. de Wit, 1998; Brown, 2006; Condie and Pease, 2008), but some authors argue that modern style subduction only began since the appearance of features such as ophiolites in the Proterozoic and

* Corresponding author. Tel.: +41 44 6328349.
E-mail address: sizova@erdw.ethz.ch (E. Sizova).

0024-4937/$ – see front matter © 2009 Elsevier B.V. All rights reserved.
doi:10.1016/j.lithos.2009.05.028

ultrahigh-pressure metamorphism in the late Neoproterozoic (Hamilton, 1998; Stern, 2005, 2007).

Based on paleomagnetic analysis and numerical modeling, O'Neil et al. (2007a,b) argue for episodic plate tectonics in the Precambrian (alternating between the active and stagnant lid regimes (cf. Sleep, 2007)), where higher mantle temperatures result in lower lithospheric stresses, causing rapid pulses of subduction interspersed with periods of relative quiescence (cf. Moresi and Solomatov, 1998). Pulses of rapid subduction would result in massive arc-volcanism and continental growth by arc-accretion—thus this mechanism predicts synchronous continental growth and fast plate velocities.

Taylor (1987) suggested that subduction became possible during the Archean-to-Proterozoic transition, representing a major change in the tectonic behavior of the lithosphere on Earth. There are many changes in both metamorphic and magmatic signatures in the geological record of the Archean-to-Proterozoic transition that have been recognized during the past decade. Based on the occurrence of both ultrahigh-temperature (UHT) and eclogite–high-pressure granulites (E–HPG) since the Archean-to-Proterozoic transition, Brown (2006, 2007) suggested this transition records the onset of a "Proterozoic plate tectonics regime". Changes in the geochemistry of Precambrian magmatic complexes are less clear-cut, which in part reflects the effect of higher mantle potential temperatures on the relationship between tectonic setting and geochemical proxies important for the identification and classification of basaltic rocks (Pearce, 2008) and in part is due to the diversity of sources and processes contributing to magma petrogenesis (e.g. Moyen, 2009). Nonetheless, there are several lines of geochemical evidence consistent with a change in geodynamics during the Mesoarchean–Neoarchean interval (e.g. Martin and Moyen, 2002; Griffin et al., 2003; Smithies et al., 2004; Martin et al., 2005), and a mantle wedge contribution to the geochemistry of magmatic rocks has been recognized since that time (e.g. Smithies et al., 2005, 2007). However, there remain a number of geologists who consider that a form of plate tectonics operated earlier in the Archean (de Wit, 1998; Watson and Harrison, 2005; Hopkins et al., 2008), and some geological observations have been interpreted to suggest that Archean subduction might have been very shallow and at low angle of dip (e.g. Abbott et al., 1994a; de Wit, 1998; Smithies et al., 2003).

It is widely accepted that the Earth has been cooling since its formation due to the decline in radiogenic heat production (e.g. Abbott et al., 1994b; Labrosse and Jaupart, 2007), although the process may not have been monotonic (e.g. Sleep, 2007). Based on the estimates of liquidus temperatures from ophiolite suites and greenstone belts, and calculations of mantle convection, upper-mantle temperature might have been about 250–180 K higher than now from the Eoarchean to the Neoarchean (Abbott et al., 1994b; Labrosse and Jaupart, 2007). Higher mantle temperatures might have had an impact on the thickness and composition of oceanic lithosphere, which in turn would have affected the rheology and tectonics of the lithosphere (e.g. Davies, 1992; de Wit, 1998; Burov and Watts, 2006; Davies, 2006; Burov and Yamato, 2008; van Hunen and van den Berg, 2008).

As a consequence of secular cooling, there is generally no modern analog to assist in understanding the tectonic style that may characterize the Precambrian, and particularly the Archean. For this reason, well-constrained numerical modeling is an appropriate tool to evaluate hypotheses based on the fragmentary evidence preserved in the geological record. To date, there are only a few systematic numerical modeling studies of Archean geodynamics or with applications to the Archean: Davies, 2006; Burov and Watts, 2006; Sleep, 2007; O'Neil et al., 2007a,b; van Hunen and van den Berg, 2008; Burov and Yamato, 2008.

There are many factors that could inhibit subduction in the Precambrian, such as higher mantle temperature, higher radiogenic heat production, the thickness of oceanic lithosphere, strongly depleted upper mantle, slab weakness, and slab breakoff (e.g. Davies, 1992; de Wit, 1998; Burov and Watts, 2006; Davies, 2006; van Hunen and van den Berg, 2008). The two important physical parameters that exhibit secular change are mantle temperature and radiogenic heat production (i.e. concentrations of radiogenic isotopes which were generally higher back in time).

Modeling by Davies (1992, 2006) with kinematically prescribed motion of oceanic plates takes into account early depletion of the upper mantle, which leads him to suggest that the ocean crust might have been thinner than on modern Earth (<3 km on average) and that the thermal boundary layer also might have been thinner overall. The thinner oceanic crust estimated from the models would substantially improve the viability of subduction, and hence of plate tectonics, in the earliest Earth. However, the numerical modeling suggests spatial and temporal variability in crustal thicknesses that might have allowed some plates to subduct whereas other plates might have been blocked to form proto continental crust.

In an alternative scenario without early depletion of the upper mantle, modeling by van Hunen and van den Berg (2008) suggests that the lower viscosity and higher degree of melting for a hotter fertile mantle might have led to both a thicker crust and a thicker depleted harzburgite layer making up the oceanic lithosphere. A thicker lithosphere might have been a serious limitation to the initiation of subduction, and a different mode of downwelling (Davies, 1992) or 'sub-lithospheric' subduction (van Hunen and van den Berg, 2008) might have characterized Earth in the Precambrian, although the conversion of basalt to eclogite may significantly relax this limitation (e.g. Ueda et al., 2008), the intrinsic lower viscosity of the oceanic lithosphere on a hotter Earth will lead to more frequent slab breakoff, and sometimes to crustal separation from the mantle lithosphere. Therefore, lithospheric weakness could be the principal limitation on the viability of modern-style plate tectonics on a hotter Earth.

The main goal of the present paper is to systematically investigate the dependence of oceanic–continental subduction on upper-mantle temperature, crustal radiogenic heat production and other parameters that could characterize the Earth in the Precambrian. Of particular interest is determining whether there is a first-order transition from the modern style of subduction to a different tectonic regime characteristic of the Archean. For this purpose, we use a newly-developed 2D coupled petrological–thermomechanical numerical model of oceanic–continental subduction. The model includes spontaneous slab bending, dehydration of subducted crust, aqueous fluid transport, mantle wedge melting, and melt extraction from the mantle to the crust resulting in crustal growth.

2. Numerical model description

2.1. Model design

2.1.1. Initial and boundary conditions

Our 2D petrological–thermomechanical numerical model simulates the processes of forced subduction of an oceanic–continental plate beneath a continental plate in a 4000 km × 200 km lithospheric/upper-mantle section (Fig. 1). The oceanic plate is 2500 km wide and is pushed toward the continent with a constant velocity of 5 cm/yr (for the reference model); the continental plate is 1500 km wide and is fixed. An imposed convergence velocity of 5 cm/yr was prescribed in a small domain in the oceanic lithosphere at the edge of the model. The rectangular staggered grid with 1001 × 101 nodal points is non-uniform. In general, the resolution of the model is 10 × 2 km, but in the center we include an area of high resolution (2 × 2 km) covering 1500 km horizontally (from $x = 1500$ km to $x = 3000$ km).

The model is based on the I2VIS code (Gerya and Yuen, 2003b) using conservative finite differences and a non-diffusive marker-in-cell technique to simulate multiphase flow. For interpolation of various parameters (density, viscosity etc.) between markers and nodes we use a distance-dependent bilinear averaging rule (Gerya and Yuen, 2003b) according to which markers located closer to a node have higher statistical weight.

In the numerical model, the oceanic crust is represented by 2 km of hydrothermally altered basalt underlain by 5 km of gabbroic rocks. The lower and upper layers of the continental crust are felsic with the total

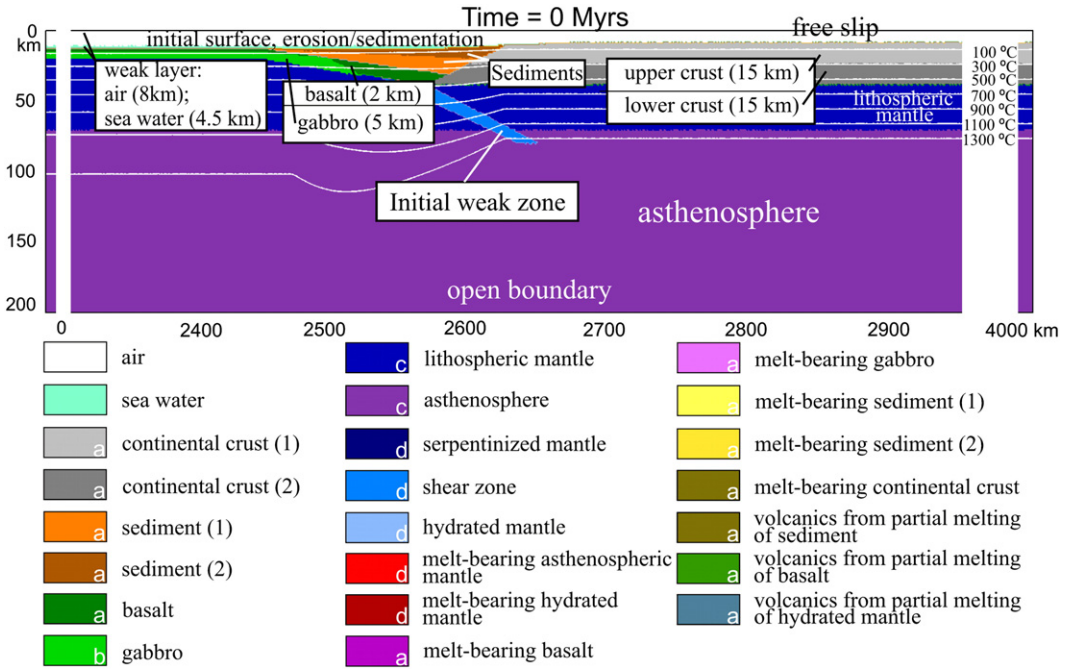

Fig. 1. Initial configuration of the numerical model (see text (2.1.1) for details). White lines are isotherms shown for increments of 200 °C starting from 100 °C. Colors indicate materials (e.g. rock type or melt) which appear in subsequent figures. For the continental crust, the sediments and the mantle two layers with the same physical properties are distinguished using different colors to better illustrate the deformation. Letters in blocks show rheology which is used for the materials (Table 1): a—wet quartzite; b—plagioclase An_{75}; c—dry olivine; d—wet olivine. The resolution of the model: at $x = 0 \div 1500$ km and $x = 3002 - 4000$ km $- 10 \times 2$ km, at $x = 1502 \div 3000$ km $- 2 \times 2$ km.

thickness 30 km. At the onset of subduction, both the lithosphere and the asthenosphere consist of anhydrous peridotite (Table 1). During the process of subduction, the mantle wedge above the slab becomes hydrated as a result of migration of fluid liberated by metamorphic reactions in the slab. The stable fluid content for each lithology was obtained by using free energy minimization (Connolly, 2005). For each lithology, the present values of radiogenic heat production are prescribed (H_r^0 in Table 1; Turcotte and Schubert, 2002).

Subduction is initiated by prescribing a weak fracture zone in the mantle with the rheology of wet olivine (Ranalli, 1995) and low plastic strength (internal friction coefficient of 0.1) between the oceanic and continental plates (e.g. Toth and Gurnis, 1998). The weak zone extends from the bottom of the continental crust to 70 km depth. Between the oceanic and the continental crust there is a prism of sediments of passive margin origin. The initial model geometry is rather idealized (e.g. a thick sedimentary wedge may not have existed before the end of the Archaean (Rey and Coltice, 2008; Flament et al., 2008)). The cooling age of the oceanic plate (which defines the initial temperature field for the plate) is 40 Ma in all experiments.

All mechanical boundary conditions are free-slip, except the lower boundary, that is permeable in the vertical direction (cf. Gorczyk et al., 2007). The top surface of the lithosphere is treated as an internal free surface by using an 8–12.5 km thick top layer (in some of the numerical experiments this thickness was increased to 18–22.5 km) with low viscosity (10^{18} Pa s) and density (1 kg/m^3 for air, 1000 kg/m^3 for sea water below $z = 10$ km level). The large viscosity contrast caused by these low viscosity boundary layers minimizes shear stresses ($<10^4$ Pa) at the top of the lithosphere making it an efficient free surface (cf. Schmeling et al., 2008). This upper boundary evolves by erosion and sedimentation according to the following Eulerian transport equation (Gerya and Yuen, 2003a; Gorczyk et al., 2007),

$$\frac{\partial z_{es}}{\partial t} = \upsilon_z - \upsilon_x \frac{\partial z_{es}}{\partial x} - \upsilon_s + \upsilon_e, \quad (1)$$

where z_{es} is a vertical position of the surface as a function of the horizontal distance x. υ_z and υ_x are the vertical and horizontal components of material velocity vector at the surface, and υ_s and υ_e are the sedimentation and erosion rates, respectively. The sedimentation and erosion rates correspond to the following relations,

$$v_s = 0 \text{ mm/y},\ v_e = v_{e0} \text{ mm/y},\ \text{when } z < z_{sea},\ \text{and}$$

$$v_s = v_{s0} \text{ mm/y},\ v_e = 0 \text{ mm/y},\ \text{when } z > z_{sea},$$

where $\upsilon_{e0} = 0.03$ mm/y and $\upsilon_{s0} = 0.03$ mm/y are the imposed erosion and sedimentation rates, respectively, and $z_{sea} = 10$ km (20 km for cases with a thicker weak top layer) is the sea-level prescribed in the model (there is neither erosion nor sedimentation at this level).

The initial temperature field for the oceanic plate is derived from the oceanic geotherm computed for the given cooling age and the upper-mantle temperature (Turcotte and Schubert, 2002). In the continental plate, the initial thermal structure corresponds to a simplified linear temperature profile limited by 0 °C at the surface and the prescribed upper-mantle temperature at 70 km depth. During numerical experiments this initial thermal structure evolves spontaneously toward a more realistic laterally variable continental geotherm controlled by local crustal thickness and radiogenic heat production as well as mantle heat flow. The initial temperature gradient in the asthenospheric mantle below 70 km depth is 0.5 °C/km. By using the reduced thickness of the continental lithosphere we follow similar numerical setups of previous authors (e.g. Regenauer-Lieb et al., 2001; Gorczyk et al., 2007) according to which subduction is initiated under a relatively thin continental margin.

2.1.2. Hydration process

In the evolution of the model, water is expelled from the subducted oceanic crust as a consequence of dehydration reactions and compaction. To account for the release of connate water by compaction, the connate water content (up to 2 wt.%) of the basaltic and sedimentary crust is specified as a linear function of depth as follows,

$$X_{H_2O(wt.\%)} = X_{H2O(p0)} \times (1 - \Delta z / 75), \quad (2)$$

Table 1
Properties of the materials used in the experiments.

Material*	ρ_0[kg/m^3](solid)	k[W/(m*K)]	Rheology/ flow law	$T_{solidus}$[K]	$T_{liquidus}$[K]	H_r [μW/ m^3]	H_L [kJ/kg]	E [kJ/mol]	n	A_D [Mpa^{-n}*s^{-1}]	V [J/(MPa*mol)]	Cohesion [MPa]	sin (φdry)
Sedimentary and felsic crust	Sediments:2600 Felsic crust: 2700	$\left[0.64+\frac{807}{(T+77)}\right]\times exp(0.00004\cdot P_{MPa})$	Wet quartzite	at P<1 $889+\frac{17900}{(P+54)}+\frac{20200}{(P+54)^2}$ at P>1200 Mpa $831+0.06\cdot P$	$1262+0.009\cdot P$	2 Felsic crust:1	300	154	2.3	$10^{-3.5}$	0	10	0.15
Melt-bearing sediments and felsic crust	2400	−//−	−//−	−//−	−//−	−//−	−//−	0	1	−//−	−//−	1	0
Basalts	3000	$\left[1.18+\frac{474}{(T+77)}\right]\times exp(0.00004\cdot P_{MPa})$	Wet quartzite	at P<1600 MPa $973-\frac{70400}{(P+354)}+\frac{77800000}{(P+354)^2}$ at P>1600 Mpa $935+0.0035\cdot P+0.0000062\cdot P^2$	$1423+0.105\cdot P$	0.25	380	154	2.3	$10^{-3.5}$	0	10	0.1
Melt-bearing basalts	2900	−//−	−//−	−//−	−//−	−//−	−//−	0	1	−//−	−//−	1	0
Gabbroic/mafic crust	3000	$\left[1.18+\frac{474}{(T+77)}\right]\times exp(0.00004\cdot P_{MPa})$	Plagioclase An_{75}	−//−	$1423+0.105\cdot P$	0.25	380	238	3.2	$10^{-3.5}$	0	10	0.6
Lithosphere-asthenosphere mantle	3300 3200(hydrated)	$\left[0.73+\frac{1293}{(T+77)}\right]\times exp(0.00004\cdot P_{MPa})$	Dry olivine	$1394+0.133\cdot P_{MP}-0.0000051\cdot P^2_{MPa}$	$2073+0.114\cdot P$	0.022	–	532	3.5	$10^{4.4}$	8	10	0.6
Hydrated mantle/ hydrated mantle in subduction zone/ serpentinized mantle	3000 (serpentinized) 3300(shear zone)	−//−	Wet olivine	Hydrated mantle: at P<1600 Mpa $973+\frac{70400}{(P+354)}+\frac{77800000}{(P+354)^2}$ at P>1600 Mpa $935+0.0035\cdot P+0.0000062\cdot P^2$	Hydrated mantle: $2073+0.114\cdot P$	0.022	Hydrated mantle: 300	470	4	$10^{3.3}$	−//−	10	0.1
Dry/melt-bearing mantle	3300/2900	−//−	Dry/wet olivine	−//−	−//−	−//−	–	0	1	$10^{4.4}$	−//−	1	0
Reference**	1,2	3	4	5	5	1	1,2	4	4	4	4,1		

ρ_0—density, k—thermal conductivity, $T_{solidus,liquidus}$—solidus and liquidus temperatures of the crust, H_r, H_L—heat production (radiogenic, latent), E—activation energy, n—stress component, A_D—material constant, V—activation volume, sin (φdry)—effective friction coefficient for dry rocks.
*For all types of rocks: C_p = 1000 J/kg, $a=3*10^{-5}$ K^{-1}, b = $1*10^{-3}$ MPa^{-1}, ** 1 = (Turcotte and Schubert, 2002), 2 = (Bittner and Schmeling, 1995), 3 = (Clauser and Huenges, 1995), 4 = (Ranalli, 1995), 5 = (Schmidt and Poli, 1998).

where $X_{H2O(p0)} = 2$ wt.% is the connate water content at the surface, and Δz is depth below the surface in km (0–75 km).

The timing of H_2O release by dehydration reactions is determined by the model physicochemical conditions and the assumption of thermodynamic equilibrium. If H_2O is found to be released in a particular location (i.e. by a particular rock marker), a fluid marker with the respective H_2O amount is generated in this location that starts to move independently with time until it reaches a lithology that assimilates H_2O. Thus, slab dehydration is achieved by setting the properties of the rock markers to values calculated for the stable mineral assemblages, whereas movement and consumption of fluid markers account for H_2O transport. To formulate this method analytically we compute the velocity of fluid markers from the local kinematical transport condition (cf. Gorczyk et al., 2007) as follows,

$$v_{x(\text{water})} = v_x, v_{z(\text{water})} = v_z - v_{z(\text{percolation})}, \quad (3)$$

where v_x and v_z are the local velocity of the mantle and $v_{z(\text{percolation})}$ is the prescribed relative velocity of upward percolation of H_2O through the mantle (10 cm/y in our experiments).

We assume an incomplete hydration of the mantle wedge as a consequence of the channelization of slab-derived fluids (cf. Davies, 1999). To account for this behavior, we arbitrarily assign 2 wt.% H_2O as an upper limit for mantle wedge hydration. For comparison, Carlson and Miller (2003) argue on the basis of seismic data that few mantle wedges achieve average H_2O contents above ~4 wt.%, whereas true H_2O saturation is predicted at ~8 wt.% (Connolly, 2005). The hydrated mantle is subdivided into two parts: an upper, serpentinized, subduction channel, and a lower, hydrated, but not serpentinized zone. The stable hydrous phases in peridotite were calculated (e.g. Gorczyk et al., 2007; Nikolaeva et al., 2008) for each P–T condition and equilibrium H_2O content ($\leq$2 wt.%).

2.1.3. Melting and extraction processes

Because the H_2O transport model does not permit complete hydration of the peridotitic mantle, the mantle solidus is intermediate between the wet and dry peridotite solidi. In reality, variable hydration would permit melting over a range of temperatures and water contents (e.g. Grove et al., 2006). To account for this behavior we assume that the degree of both hydrous and dry melting is a linear function of pressure and temperature (Johannes, 1985; Schmidt and Poli, 1998; Poli and Schmidt, 2002). In this model the standard (i.e. without melt extraction) volumetric degree of melting M_0 is,

$$M_0 = \begin{cases} 0 & T < T_{\text{solidus}} \\ \dfrac{T - T_{\text{solidus}}}{T_{\text{liquidus}} - T_{\text{solidus}}} & T_{\text{solidus}} < T < T_{\text{liquidus}}, \\ 1 & T > T_{\text{liquidus}} \end{cases} \quad (4)$$

where T_{solidus} and T_{liquidus} are, respectively, the solidus temperature (wet and dry solidi are used for the hydrated and dry mantle, respectively) and the dry liquidus temperature at a given pressure and rock composition (Table 1). To simulate melt extraction from melt-bearing rocks we define a melt extraction threshold $M_{\max}$ (4 wt.%) and a non-extractable amount of melt $M_{\min} < M_{\max}$ that will remain in the source. The influence of these parameters on subduction dynamics and crustal growth is investigated for the case of constant $M_{\max}/M_{\min} = 2$.

The amount of melt extracted during the evolution of each experiment is tracked by markers. The total amount of melt, M, for every marker takes into account the amount of previously extracted melt and is calculated as,

$$M = M_0 - \sum_n M_{\text{ext}}, \quad (5)$$

where $\sum_n M_{\text{ext}}$ is the total melt fraction extracted during the previous n extraction episodes. According to our model the rock is considered refractory when the extracted melt fraction is bigger than the standard one (i.e. when $\sum_n M_{ext} > M_0$). Once the total amount of melt, M, computed from Eqs. (4) and (5) for a given marker exceeds $M_{\max}$, the extractable melt fraction $M_{\text{ext}} = M - M_{\min}$ is assumed to migrate upward and the value of $\sum_n M_{\text{ext}}$ is updated. We assume that melt migration is rapid compared to the deformation of unmelted mantle, so that the velocity of the melt is independent of mantle dynamics (Elliott et al., 1997; Hawkesworth et al., 1997). Thus, the extracted melt is transported instantaneously to the surface forming new volcanic crust above the extraction area.

2.1.4. Rheological model

The effective creep viscosities of rocks are represented as a function of temperature and stress by experimentally determined flow laws (Table 1). The viscosity for dislocation creep depends on strain rate, pressure and temperature and is defined in terms of deformation invariants (Ranalli, 1995) as follows,

$$\eta_{\text{creep}} = (\dot{\varepsilon}_{\text{II}})^{(1-n)/n} F(A_D)^{-1/n} exp\left(\frac{E + VP}{nRT}\right), \quad (6)$$

where $\dot{\varepsilon}_{II} = \sqrt{1/2\,\dot{\varepsilon}_{ij}\,\dot{\varepsilon}_{ij}}$ is the second invariant of the strain rate tensor and A_D, E, V and n are the experimentally determined flow law parameters (Table 1), the material constant, the activation energy, the activation volume and the stress exponent, respectively. F is a dimensionless coefficient depending on the type of experiments on which the flow law is based and is used for conversion of experimentally determined rheologies to model stress states. For example, $F = \frac{2^{(1-n)/n}}{3^{(1+n)/2n}}$ for triaxial compression, and $F = 2^{(1-2n)/n}$ for simple shear.

Small melt fractions are known to significantly change the effective viscosity of partially melted rocks (e.g. Kohlstedt and Zimmerman, 1996; Rosenberg and Handy, 2005; Holtzman and Kohlstedt, 2007). In our experiments, effective rock viscosity in melt-bearing regions computed with Eq. (6) was always close to the lower cut-off viscosity value (10^{17} Pa s). Therefore, for simplicity we applied Eq. (6) for both solid and melt-bearing rocks (the maximum melt fraction in our experiments was limited to no more than 4 wt.% by melt extraction).

The ductile rheology of rocks is combined with a brittle rheology to yield an effective visco-plastic rheology. For this purpose the Mohr-Coulomb yield criterion (Ranalli, 1995) is implemented by limiting creep viscosity, η_{creep}, as follows,

$$\eta_{\text{creep}} \leq \frac{\sigma_{\text{yield}}}{2\dot{\varepsilon}_{\text{II}}}, \quad (7)$$

$$\sigma_{\text{yield}} = c + P\sin(\varphi), \quad (8)$$

$$\sin(\varphi) = \sin\left(\varphi_{\text{dry}}\right)\lambda_{\text{fluid}}, \text{ and} \quad (9)$$

$$\lambda_{\text{fluid}} = 1 - \frac{P_{\text{fluid}}}{P_{\text{solid}}}. \quad (10)$$

Thus, the plastic strength depends on the mean stress on the solids, $P_{\text{solid}} = P$ (dynamic pressure), the cohesion, c, which is the strength at $P = 0$, and on the effective internal friction angle, φ, which is calculated from the friction angle of dry rocks, φ_{dry}, and the pore fluid pressure factor λ_{fluid}. This factor is interpreted as $\lambda_{\text{fluid}} = 1 - \frac{P_{\text{fluid}}}{P_{\text{solid}}}$; the pore fluid pressure P_{fluid} reduces the yield strength σ_{yield} of fluid-containing porous or fractured media. In our numerical experiments λ_{fluid} was varied from 0 to 1. Similarly, the weakening effect of ascending melts is included. During a melt extraction episode, the yield strength σ_{yield} of rock in the column between the source of the melt and the surface is decreased according to λ_{melt}, which was also varied from 0 to 1. In the first series of numerical experiments we used low values of $\lambda_{\text{fluid}} = 0.001$ and $\lambda_{\text{melt}} = 0.001$ providing significant weakening of rocks subjected to free fluid/melt propagation and creating favorable conditions for realistic one-sided subduction (Gerya et al., 2008a).

Table 2
Experimental results for varied mantle temperature and crustal radiogenic heat production showing the different regimes.

	ΔT=0 K	ΔT=50 K	ΔT=100 K	ΔT=150 K	ΔT=160 K	ΔT=175 K	ΔT=200 K	ΔT=250 K
$H_r=H_r^0$	The reference model					Transitional regime		
$H_r=1.5^*H_r^0$								
$H_r=2^*H_r^0$		"Modern subduction" regime				"Pre-subduction" regime		"No-subduction" regime
$H_r=2.5^*H_r^0$								
$H_r=3^*H_r^0$								
$H_r=5^*H_r^0$								

ΔT — difference between the prescribed upper-mantle temperature and the present value of 1360 °C at 70 km depth; H_r^o — present value of average crustal radiogenic heat production, H_r — prescribed value of average crustal radiogenic heat production. Experiments show two first order transitions between tectonic regimes (their boundaries are shown with bold lines) (see text (3.2.) for details). At ΔT = 175 K and close to present values of radiogenic heat production a transitional regime between the "modern subduction" and the "pre-subduction" regime occurs.

According to our rheological model, the major parameters controlling effective viscosity of rocks at relatively cold temperatures are the weakening effects of fluids and melts (Eqs. (7)–(10)). On the other hand, the temperature- and stress-dependencies of viscosity are the dominant rheological factors (Eq. (6)) for hot rocks. 10^{17} and 10^{25} Pa s are the lower and upper cut-off values for the viscosity of all types of rocks in our numerical experiments.

2.1.5. Conservation equations

The model includes 2D creeping flow with thermal and chemical buoyancy forces as well as mechanical heating as introduced by the heat conservation equation (Eq. (11)) for which the extended Boussinesq approximation (Christensen and Yuen, 1985) is used, as follows,

$$\rho C_P\left(\frac{DT}{Dt}\right) = -\frac{\partial q_x}{\partial x} - \frac{\partial q_z}{\partial z} + H_r + H_a + H_s + H_L, \quad (11)$$

$$q_x = -k(T,P,C)\frac{\partial T}{\partial x}, \quad (12)$$

$$q_z = -k(T,P,C)\frac{\partial T}{\partial z}, \text{ where} \quad (13)$$

H_r = constant (dependent on rock composition),

$$H_a = T\alpha\left(v_x\frac{\partial P}{\partial x} + v_z\frac{\partial P}{\partial z}\right), \text{ and} \quad (14)$$

$$H_s = \sigma_{xx}\dot{\varepsilon}_{xx} + \sigma_{zz}\dot{\varepsilon}_{zz} + 2\sigma_{xz}\dot{\varepsilon}_{xz}. \quad (15)$$

The effect of latent heating due to equilibrium melting/crystallization is included implicitly by increasing the effective heat capacity (C_{Peff}) and the thermal expansion (α_{eff}) of the melting/crystallizing rocks ($0<M<1$, Eq. (4)), calculated as (Burg and Gerya, 2005):

$$C_{Peff} = Cp + H_L\left(\frac{\partial M}{\partial T}\right)_{P=\text{const}}, \quad (16)$$

$$\alpha_{eff} = \alpha + \rho\frac{H_L}{T}\left(\frac{\partial M}{\partial P}\right)_{T=\text{const}}, \quad (17)$$

where Cp is the heat capacity of the solid rock and H_L is the latent heat of melting of the rock (Table 1).

The 2D continuity equation with time-dependent density describes the conservation of mass for a compressible fluid (Gerya and Yuen, 2007), as follows,

$$\frac{\partial v_x}{\partial x} + \frac{\partial v_z}{\partial z} = -\frac{1}{\rho}\frac{D\rho}{Dt}, \quad (18)$$

where $\frac{D\rho}{Dt}$ is the substantive density time derivative which accounts locally for melt extraction.

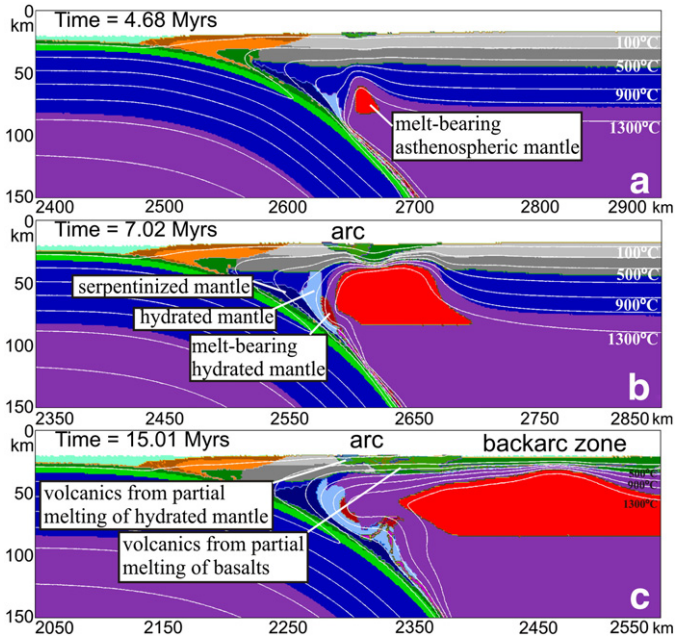

Fig. 2. Evolution of the reference model. The model presents a retreating one-sided oceanic–continental subduction with the formation of a mantle wedge, a magmatic arc (b,c) and an extensional backarc basin with newly-forming oceanic floor (c) (see text for details).

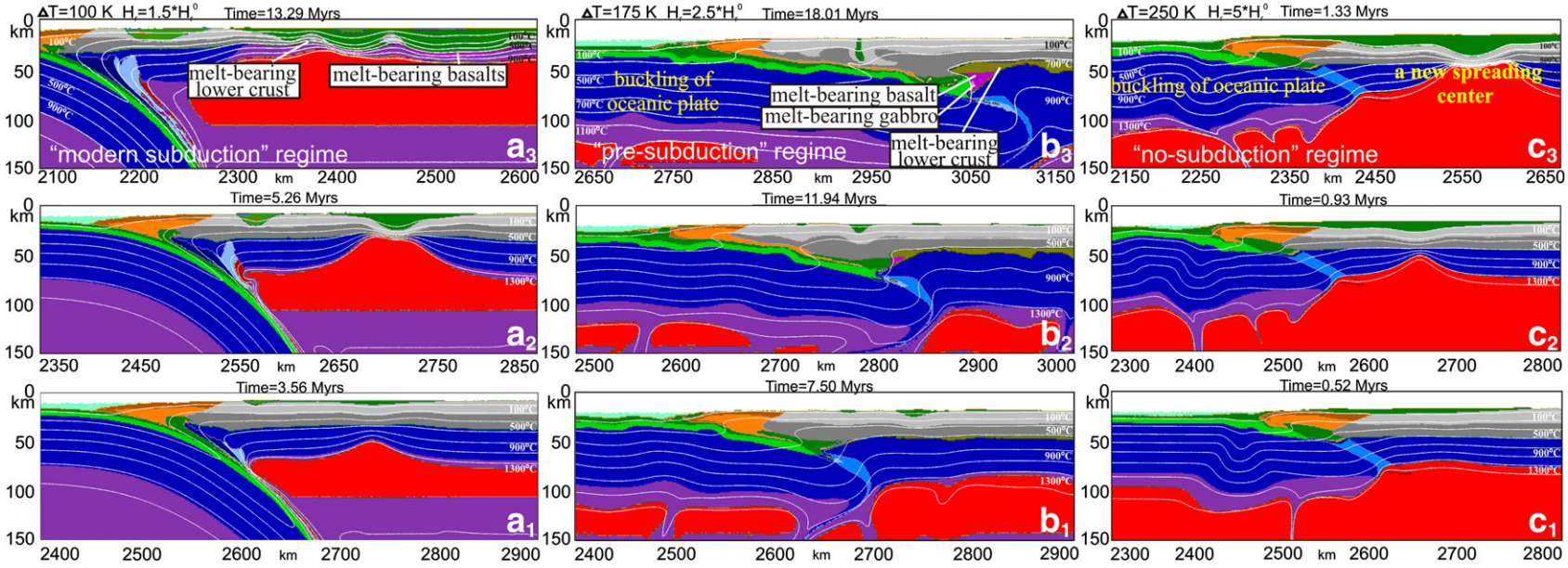

Fig. 3. Evolution of numerical experiments independently varying the upper-mantle temperature and the crustal radiogenic heat production (a,b,c). Experiments show three different tectonic regimes: (a)—"modern subduction" regime ($\Delta T = 0$–175 K), (b)—"pre-subduction" regime ($\Delta T = 175$–250 K) and (c)—"no-subduction" regime ($\Delta T \geq 250$ K). Lower boundary of melt-bearing asthenospheric mantle (red areas) in (a), and (b) is located at depths of 100–150 km while in (c) this boundary extends to depths of >200 km (i.e. below the bottom of the model).

For creeping flow, all inertial terms may be neglected and the Stokes equations for slow flow in 2D are as follows,

$$\frac{\partial \sigma_{xx}}{\partial x} + \frac{\partial \sigma_{xz}}{\partial z} = 0, \text{ and} \tag{19}$$

$$\frac{\partial \sigma_{xz}}{\partial x} + \frac{\partial \sigma_{zz}}{\partial z} = \frac{\partial P}{\partial z} - g\rho(T,P,C,M). \tag{20}$$

The components of the deviatoric stress tensor are calculated using the viscous constitutive relationship between stress and strain rate for a compressible fluid (Gerya and Yuen, 2007), as follows,

$$\sigma_{ij} = 2\eta\dot{\varepsilon}_{ij}, \tag{21}$$

$$\dot{\varepsilon}_{xx} = -\dot{\varepsilon}_{zz} = \frac{1}{2}\left(\frac{\partial v_x}{\partial x} - \frac{\partial v_z}{\partial z}\right), \text{ and} \tag{22}$$

$$\dot{\varepsilon}_{zx} = \dot{\varepsilon}_{xz} = \frac{1}{2}\left(\frac{\partial v_x}{\partial z} + \frac{\partial v_z}{\partial x}\right), \tag{23}$$

where the effective viscosity η is dependent on composition, temperature, pressure and strain rate.

The governing equations are solved with the I2VIS code (Gerya and Yuen, 2003b), which combines a conservative finite difference method with a non-diffusive-marker-in-cell technique.

2.2. Modeling procedure

Ideally, models to examine tectonics in the Precambrian should include many of the parameters that may be different from the present day. Here we restrict our modeling to an investigation of the variation in the most likely controlling parameters, as suggested in the literature for the Precambrian.

To start our investigation we began with a reference model that reproduces the stable one-sided subduction typical of modern subduction (cf. Gerya et al., 2008a) using the following parameters typical of Earth at present: mantle temperature of 1360 °C at 70 km depth; crustal heat production, H_r^0, from Turcotte and Schubert (2002); thickness of oceanic crust of 7 km and continental crust of 30 km; and, a constant convergence velocity of the oceanic plate of 5 cm/yr. Based on this reference model we performed 48 numerical experiments by independently varying mantle temperatures and crustal radiogenic heat production (Table 2). We varied the upper-mantle temperature from 1360 °C (present day) to 1610 °C at 70 km depth by 50 °C increments, plus two intermediate steps at 1520 °C and 1535 °C. The difference between a model temperature and the present day value will be denoted as ΔT. Radiogenic heat production is varied from present day values (H_r^0) to values up to 5 times higher ($H_r = 5 * H_r^0$).

A second series of experiments was performed under conditions of simultaneous increase in upper-mantle temperature and radiogenic heat production to test the rheological influence of fluid and melt on the tectonic regime. For the initial experiments we used the maximum weakening effect of fluids and melts ($\lambda_{fluid} = \lambda_{melt} = 0.001$; Eq. (8)). In these experiments, we also increased the thickness of the air layer to 18 km to allow thick oceanic crust to be formed at the surface, which is a relevant process for sufficiently hot models characterized by intense dry mantle melting.

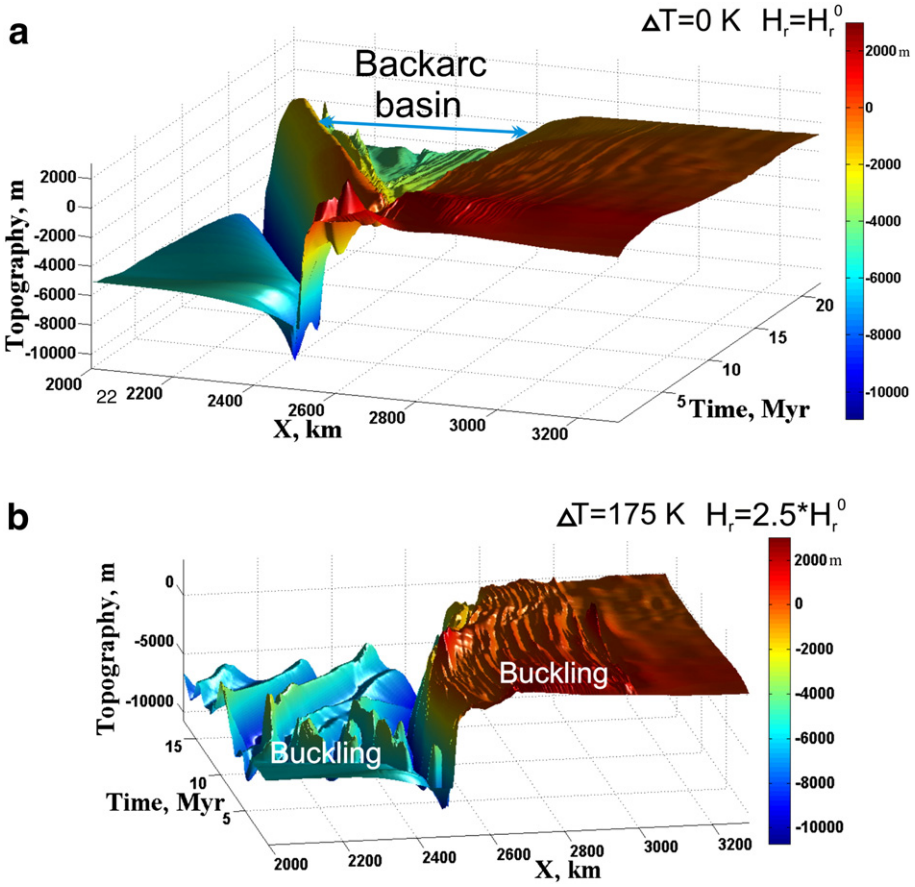

Fig. 4. Topographic evolution of numerical experiments for the "modern subduction" regime (a) and the "pre-subduction" regime (b). For the first regime, the trench retreats forming the backarc basin, whereas for the second regime, only buckling of the plates is observed.

Other experiments were undertaken to evaluate the influence on the subduction regime of the following parameters as the upper-mantle temperature was increased: the thickness of the oceanic crust ($d=7$, 10, 15, 20 km); the density contrast between continental and oceanic lithospheric mantle ($\Delta c=25$, 50, 75 kg/m^3); the prescribed convergence velocity of the oceanic plate toward the continent ($V=2$, 5, 10, 15 cm/yr); and, phase transformations. The influence of the presence of an initial weak fracture zone on the initiation of subduction has been also explored. For this investigation experiments were run with different $\Delta T=0$, 100, (150 in some cases), 200, and 250 K and normal radiogenic heat production.

3. Numerical experiments

3.1. The reference model of present-day subduction

The reference model refers to the present upper-mantle temperature and crustal radiogenic heat production; it produces a typical retreating one-sided oceanic–continental subduction with formation of a mantle wedge, magmatic arc and extensional backarc basin with newly forming oceanic floor (Fig. 2). When the oceanic plate reaches 70 km depth it starts to dehydrate, which leads to hydration and wet melting of the mantle above the slab. In accordance with the high degree of magmatic weakening adopted ($\lambda_{melt}=0.001$), ascent toward the surface of melts extracted from the melt-bearing wet mantle wedge strongly weakens the lithospheric mantle above the wedge. This weakening results in extensional necking of the overriding plate and the rise of hot and dry mantle asthenosphere into the necks as the trench is pulled back by the retreating slab. Subsequent decompression melting of positively buoyant rising asthenospheric mantle further stabilizes the extension process. All these processes lead to the growth of a magmatic arc (3–4 Ma after beginning of subduction) at the surface of the continental plate. The new volcanic crust consists of various magmatic rocks formed by partial melting of hydrated (flux melting above the slab) and anhydrous (decompression melting in the rising asthenosphere) mantle, subducted oceanic crust and subducted sediments.

As the trench retreats the melt-bearing asthenosphere rises to trigger thinning of the continental crust, forming an intra-arc spreading center leading to splitting of the arc and development of a backarc basin (after 5–6 Ma). The formation of a spreading center accelerates trench retreat since it acts as a break in the overriding plate. Tha appearance of a melt-bearing mantle region below the spreading center (cf. broad red region in Fig. 2c) is driven by decompression melting. The new oceanic crust consists of basalts up to 10 km thick generated by decompression melting of dry mantle

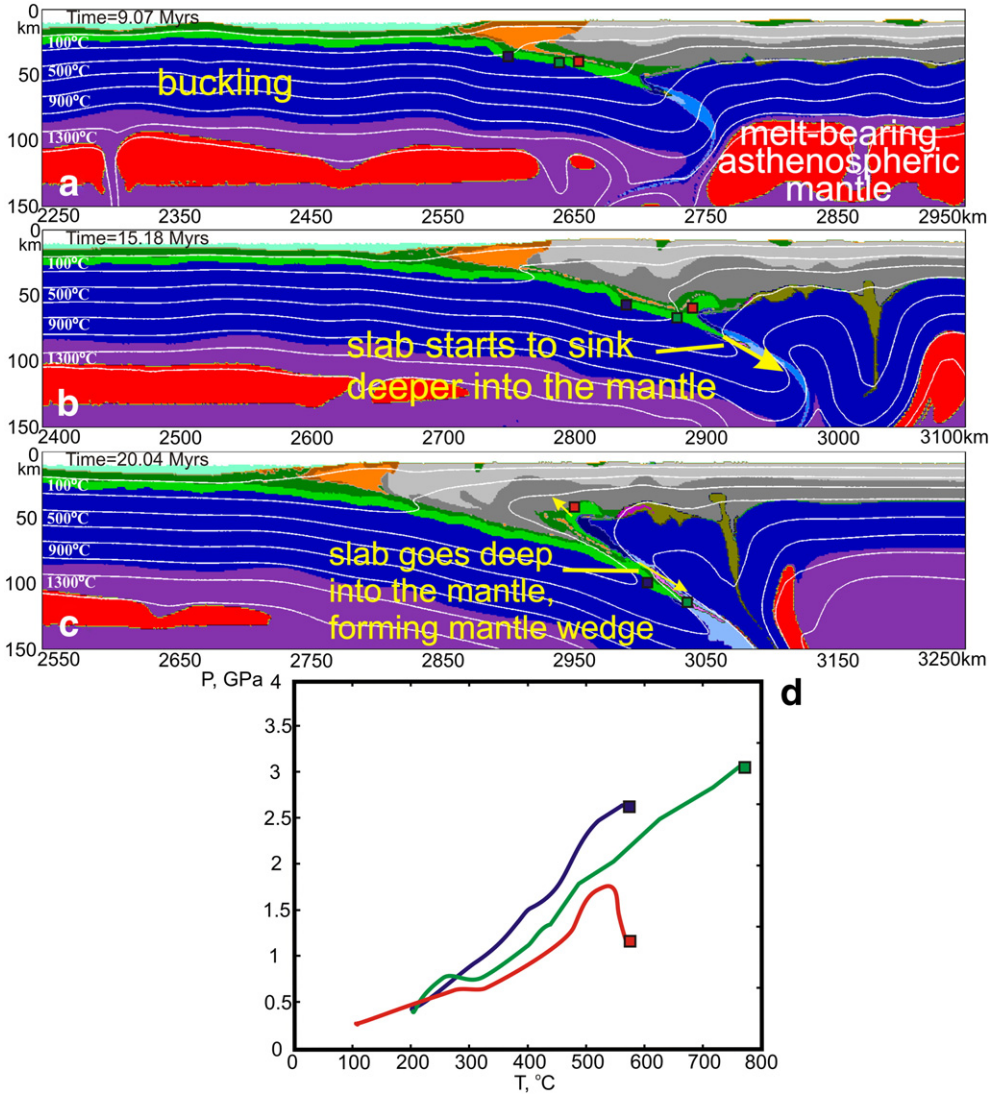

Fig. 5. Evolution of the numerical experiment in which the tectonic regime evolves from the "pre-subduction" (a,b) to the "modern subduction" (c) regime (i.e. underthrusting transforms to subduction). The squares on the snapshots refer to the diagram with the *P*–*T* paths (d). The experiment was performed at $\Delta T=175$ K and $H_r=1.5*H_r^o$.

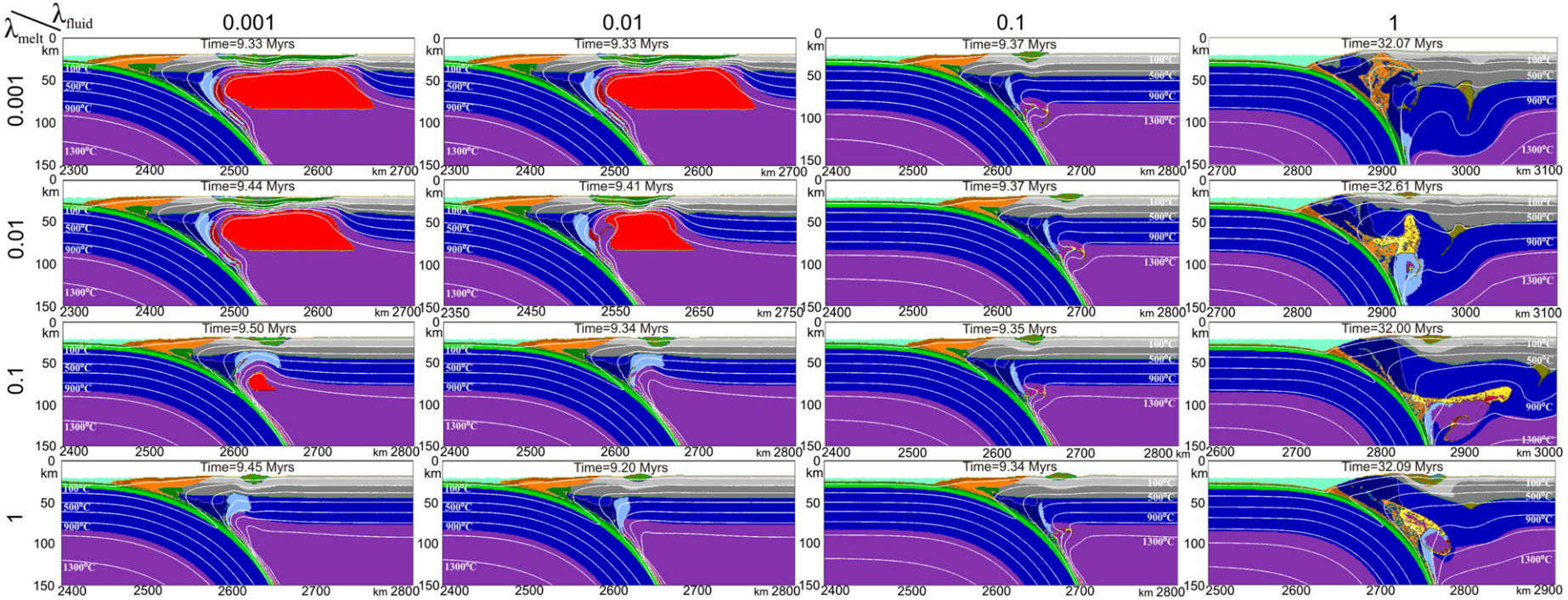

Fig. 6. Snapshots from numerical experiments in which the fluid and melt weakening factors (λ_{fluid} and λ_{melt}) are varied independently for the reference model. Snapshots of the experiments with $\lambda_{fluid} = 1$ are made for the time step 32 Myrs, whereas for the other experiments the snapshots are made for the time step 9 Myrs.

asthenosphere rising into this break, similar to processes acting at mid-ocean ridges. With the exception of this rising fertile asthenospheric mantle, the melt fraction in the melt-bearing mantle region remains below the extraction threshold (i.e. below 4%). The topographic evolution shows very clearly the growth of the magmatic arc and the extension in the newly created backarc basin (Fig. 4a).

3.2. Influences of mantle temperature and crustal radiogenic heat production

Based on the numerical experiments with independently varying mantle temperature and crustal radiogenic heat production, we identify two changes in tectonic style that bracket a transitional tectonic regime (Table 2). From low temperature to high temperature we call the three tectonic regimes: the "modern subduction" regime, the "pre-subduction" regime, and the "no-subduction" regime. Our experiments show that changes in the upper-mantle temperature play a dominant role in causing these transitions, whereas crustal radiogenic heat production plays only a minor role.

"Modern subduction" is a tectonic regime with a characteristic style of stable one-sided subduction similar to the reference model. This regime is observed over a wide range of mantle temperatures (ΔT = 0–160 K) irrespective of crustal radiogenic heat production (Table 2).

Increasing both mantle temperature and radiogenic heat production leads to larger amounts of mantle melting and newly formed oceanic crust in the backarc basin. The location of the backarc basin also changes; with increasing upper-mantle temperature, the backarc basin forms further from the arc. Both basalts and lower continental crust in the backarc basin start to melt in response to rise of hot asthenospheric mantle (e.g. Fig. 3a).

At ΔT = 175 K, we observe a transition to a different tectonic regime, which we term "pre-subduction" (Table 2). In contrast to "modern subduction", this regime is observed in a narrow range of upper-mantle temperature (ΔT = 175–250 K) for almost the whole range of crustal radiogenic heat production.

Under this tectonic regime, plates are internally deformable because they are rheologically weakened by intense percolation of melts continuously generated from the underlying hot melt-bearing sub-lithospheric mantle. Convergence results in shallow underthrusting of the continental plate by the oceanic plate (Fig. 3b). The oceanic plate may underthrust quite far under continental crust (to 200 km) displacing and folding the continental lithosphere. Due to the intense extraction of melts, the thickness of oceanic basalts becomes about three times larger. In contrast to the present subduction regime, there is no formation of a mantle wedge or a backarc basin, which is reflected in the development of topography (Fig. 4b). The velocity of the slab is very low and therefore it heats up markedly during underthrusting which leads to melting of the frontal zones of both oceanic and lower continental crust and to the formation of contrasting volcanic rocks at the surface.

Details of the transitional behavior between the "pre-subduction" and the "modern subduction" regimes may be observed in Fig. 5, representing a model with lowered radiogenic heat production ($H_r = 1.5 * H_r^0$) and a transitional value of the mantle temperature (ΔT = 175 K). From the beginning of the experiment, underthrusting occurs, and the oceanic plate is underthrusted for 100–150 km horizontally under the continental plate (for about 13 Ma) by displacing and buckling the continental lithospheric mantle. At this point, the oceanic slab starts to sink into the mantle in a "two-sided subduction" mode; both the oceanic plate and the buckled continental lithospheric mantle subduct together in an asymmetric manner (cf. Gerya et al., 2008a). Part of the oceanic crust separates from the slab at a depth of about 50 km and begins to move upward (Fig. 5) which could result in the formation and exhumation of high-pressure (eclogitic) metamorphic rocks (see 4.3. for details and discussion).

Further increase in the upper-mantle temperature above ΔT = 250 K causes a transition from the "pre-subduction" regime to a "no-subduction" regime. At this stage, horizontal movements are predominant and are accommodated by internal strain; even shallow underthrusting does not occur under the imposed convergence (Fig. 3c). Plates are extremely weak and easily deformed internally; the continental plate is commonly fragmented by new spreading centers rapidly forming in many locations and producing large amounts of volcanic rocks (basalts) due to decompression melting of anhydrous mantle.

Thus, the first transition at ΔT = 160–175 K above the present temperature is quite sharp while the second (ΔT = 200–250 K) is not. The crucial difference between the "modern subduction" and the "pre-subduction" regimes consists of the presence of a layer of hot rapidly convecting melt-bearing sub-lithospheric mantle, which continuously produces melts percolating upward and weakening the overlying lithosphere.

3.3. Influence of lithospheric weakening by fluids and melts

To check the influence of slab-derived fluids and sub-lithospheric melts on changes in tectonic regime, we performed another series of numerical experiments with independently varied fluid and melt

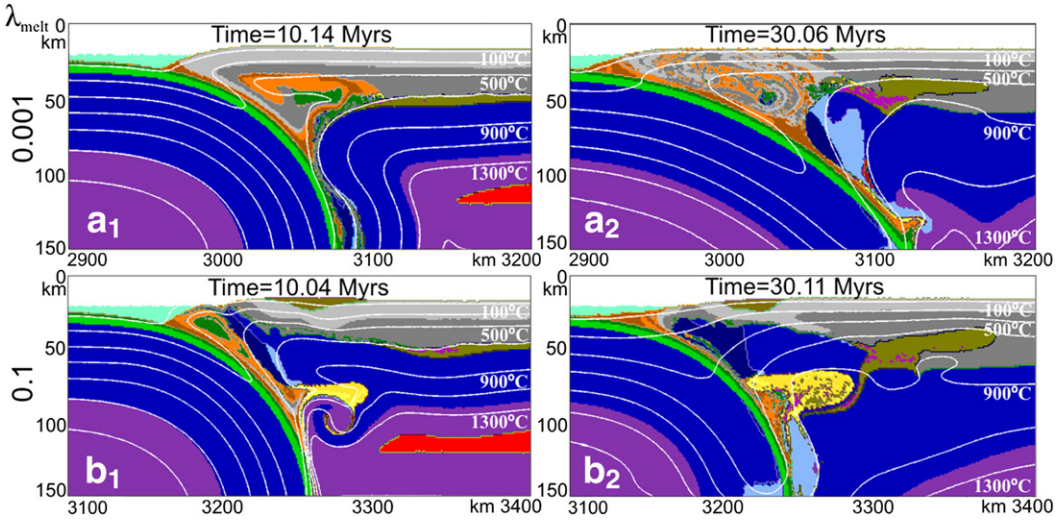

Fig. 7. Evolution of numerical experiments with melt weakening (λ_{melt}) equals 0.001 and 0.1 at λ_{fluid} = 1 for the "modern subduction" regime (ΔT = 100 K, $H_r = 2 * H_r^0$). Two time steps for each experiment are shown. In both experiments strong subduction erosion is observed. At λ_{melt} = 0.1, a plume of melt-bearing sediments forms below the overriding plate.

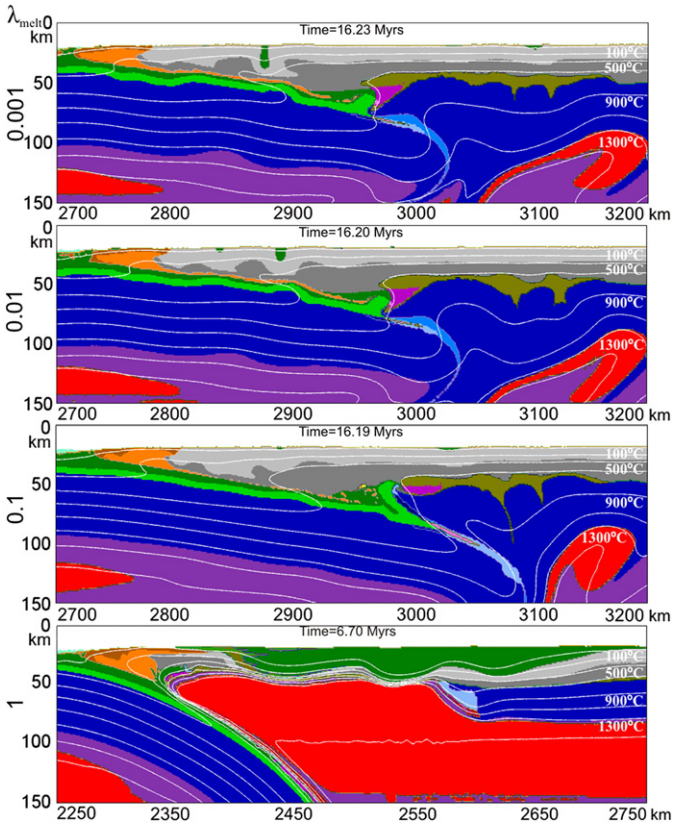

Fig. 8. Snapshots from numerical experiments with varied melt weakening (λ_{melt}: 0.001–1) at constant $\lambda_{fluid}=0.001$ for the "pre-subduction" regime ($\Delta T=200$ K, $H_r=2.75*H_r^0$). Increasing λ_{melt} (hence, increasing plate strength) leads to a transition from the "pre-subduction" regime to the "modern subduction" regime at $\lambda_{melt}>0.1$.

weakening factors λ_{fluid} and λ_{melt} (Eq. (10)). Since the exact degree of fluid- and melt-related weakening are unknown we explored a wide range of λ_{fluid} and λ_{melt} (0.001, 0.01, 0.1, 1) for five pairs of mantle temperature and radiogenic heat production taken from the first series of experiments ($\Delta T=0$ K, $H_r=H_r^0$; $\Delta T=100$ K, $H_r=2*H_r^0$; $\Delta T=200$ K, $H_r=1.5*H_r^0$; $\Delta T=200$ K, $H_r=2.75*H_r^0$; $\Delta T=250$ K, $H_r=3.5*H_r^0$).

First, we checked the influence of λ_{fluid} and λ_{melt} on the reference model. At low λ_{fluid} , low λ_{melt} values favor dry mantle melting, backarc extention and the production of backarc oceanic crust (Fig. 6). The variation in λ_{melt} does not change the style of subduction although the velocity of the process becomes slower with a stronger continental plate resulting from the higher λ_{melt} values. In contrast, fluid related weakening greatly affects the style of subduction. With increasing λ_{fluid} (i.e. decreasing the weakening effect of slab-derived fluids), stronger coupling between the subducting and the overriding plate occurs, resulting in less mantle wedge melting and strong compression and shortening of the continental plate. The shortening precludes the development of an arc or a backarc basin (at $\lambda_{fluid}=0.1$), and allows the inception of two-sided subduction at $\lambda_{fluid}=1$. At high values of λ_{fluid}, we also observe strong subduction erosion of sediments, resulting in the reduced size and even disappearance of the accretionary prism. In the case of $\lambda_{melt}=0.01$, after 32 Ma, and after the beginning of subduction, melt-bearing subducted sediments detach from the slab and form a compositionally buoyant plume (e.g. Gerya and Yuen, 2003a; Gerya et al., 2006), whereas at $\lambda_{melt}=0.1$, after 6 Ma the subducted sediments start to move below the continental lithosphere and not upward (Fig. 6).

Very similar results are observed for hotter experiments but still within the "modern subduction" regime ($\Delta T=100$ K; $H_r=2*H_r^0$). There are indeed some differences for high values of λ_{fluid} ($\lambda_{fluid}=1$; Fig. 7). These experiments at $\lambda_{melt}=0.001$–0.01 are initially characterized by a two-sided subduction, which may evolve at a later stage toward a one-sided subduction (Fig. 7a_1,a_2). Similar to the "modern subduction" regime at lower upper-mantle temperatures, two competing tendencies are observed due to the strong coupling between plates and subduction erosion of sediments (cf. Figs. 7 and 6, $\lambda_{fluid}=1$): (i) in the early stages of subduction bending of the continental mantle lithosphere produces generally two-sided subduction (Fig. 7a_1); (ii) the formation of a plume of melt-bearing positively-buoyant subducted sediments that delaminate from the slab and flow below the overriding plate during a transition to one-sided subduction (Fig. 7b_1,b_2).

In contrast to the "modern subduction" regime, which is mainly affected by a fluid-related weakening, in the "pre-subduction" regime, the weakening effects of sub-lithospheric melts are crucial (Fig. 8). An increase in λ_{melt} and consequently lithospheric strength leads to a transition from a "pre-subduction" to the "modern subduction" regime at $\lambda_{melt}>0.1$ (Fig. 8). After this transition underthrusting does not form and a rapidly retreating oceanic plate sinks into the mantle. In this hot

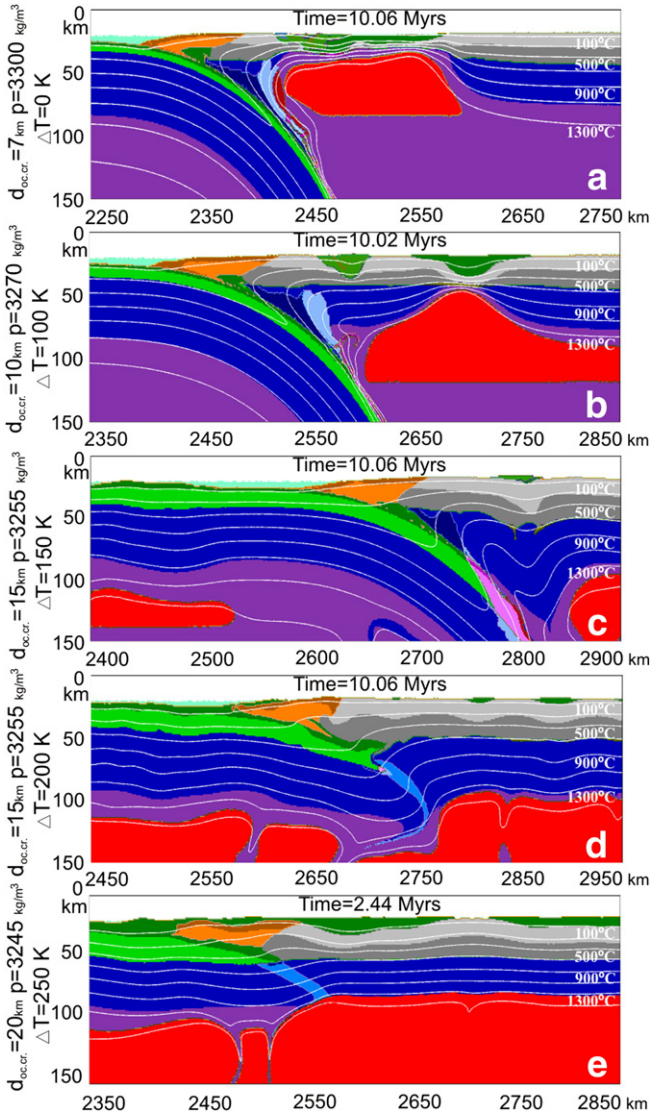

Fig. 9. Snapshots from numerical experiments with varied thickness of the oceanic crust ($d_{oc.cr.}$), lower standard density of the lithospheric mantle (ρ) and upper-mantle temperature. The increase in the oceanic crust thickness is accompanied by a decrease in the lithospheric mantle density and an increase in the upper-mantle temperature. Fig. 10a–10c corresponds to the "modern subduction" regime, 10d to the "pre-subduction" regime and 10e to the "no-subduction" regime.

one-sided subduction regime, fluid-related weakening influences the model behavior in the same way as in the case of "modern subduction". Particularly, at maximal values of λ_{fluid} and λ_{melt} a backarc basin is not developed and collisional two-sided subduction occurs with sediments mixing with the frontal zone of the continental crust in a similar fashion to the "modern subduction" regime (Fig. 7).

The "no-subduction" regime characterized by weak fragmented plates is not affected by fluid related weakening but demonstrates a tendency toward the "pre-subduction" regime behaviour with increasing λ_{melt} and strength and coherency of the plates. This change is expressed in the decreasing number of new spreading centers and in the notable underthrusting of the oceanic plate under the continent at high values of $\lambda_{melt} \geq 0.1$.

Results with variable λ_{fluid} and λ_{melt} further confirm that transitions between different regimes are mainly controlled by the rheological influence of sub-lithospheric melts. Percolation of these melts strongly weakens the overlying plates and makes them internally deformable, which in turn precludes one-sided modern-style subduction (Gerya et al., 2008a) and defines a transition to the "pre-subduction" and even the "no-subduction" regimes that may be characteristic for hotter Earth.

3.4. Sensitivity of the model to other parameters

3.4.1. Influence of oceanic crust thickness and eclogitization

A common point of view concerning the possible absence of plate tectonics in the Precambrian is the inhibition of subduction by increased buoyancy of the oceanic lithosphere due to the thicker oceanic crust and higher degree of lithospheric mantle depletion. Here we tested this possibility by exploring thicker oceanic crust (10–20 km) and lower standard density of the lithospheric mantle (3245–3270 kg/m^3, dark blue layer in Fig. 9) at elevated mantle temperature ($\Delta T = 100$, 200, and 250 K, Fig. 9) corresponding to Precambrian conditions. For the "pre-subduction" regime ($\Delta T = 200$ K) we also performed additional experiments with variable thickness of oceanic crust (Fig. 10). This test is rather simplified since in nature the thickness of the depleted oceanic mantle should also positively correlate with the thickness of the oceanic crust.

Under the prescribed conditions of plate convergence increasing the thickness of oceanic crust does not affect changes between the three tectonic regimes observed in the experiments: the transition from the "modern subduction" regime to a "pre-subduction" regime still occurs at about $\Delta T = 200$ K, whereas above about $\Delta T = 250$ K the

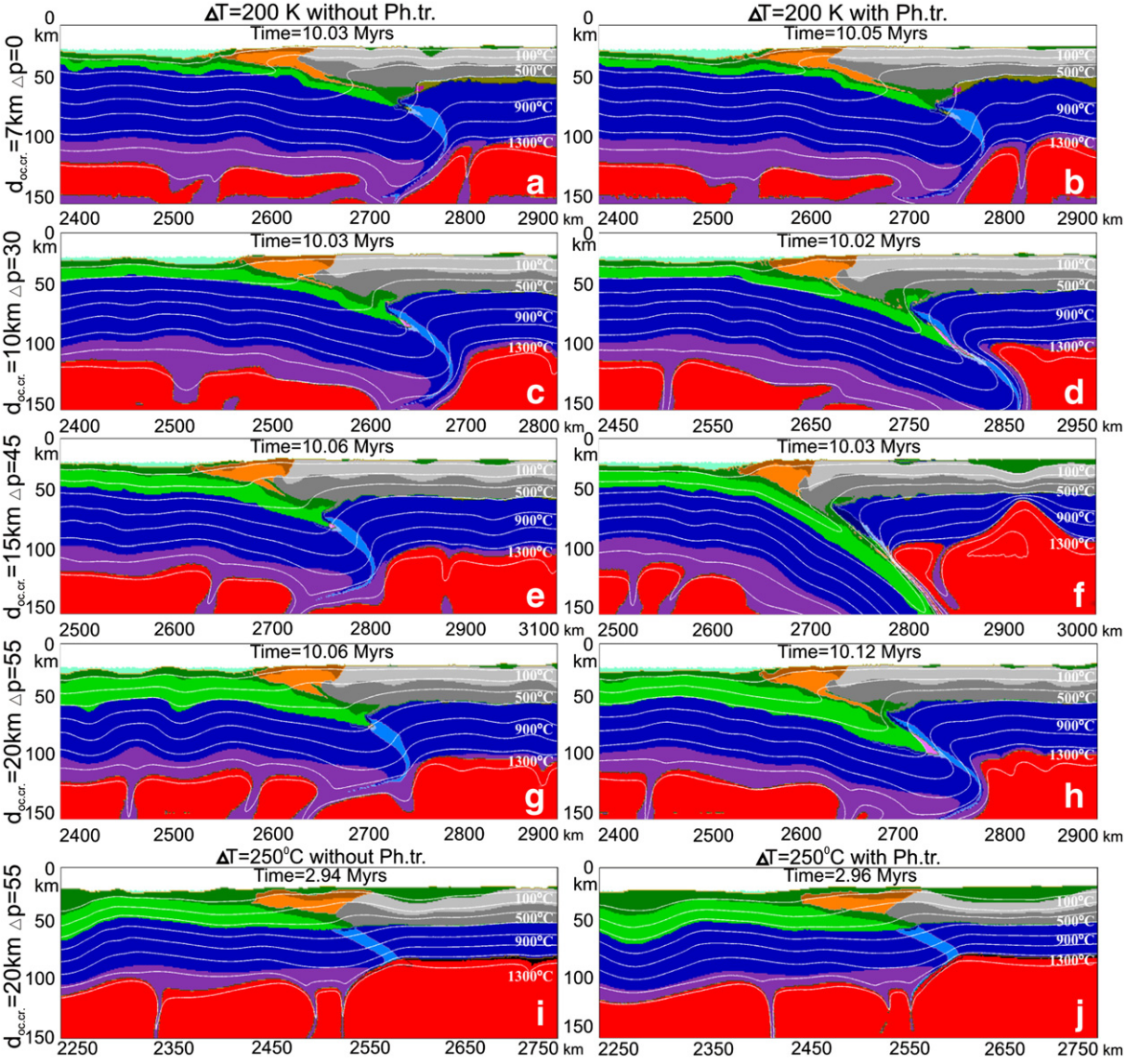

Fig. 10. Snapshots from numerical experiments with varied thickness of the oceanic crust ($d_{oc.cr.}$) and lower standard density for the lithospheric mantle (ρ) at mantle temperatures of $\Delta T = 200$ and 250 K: a,c,e,g,i—without phase transformations; b,d,f,h,j—phase transformations included (see text for details).

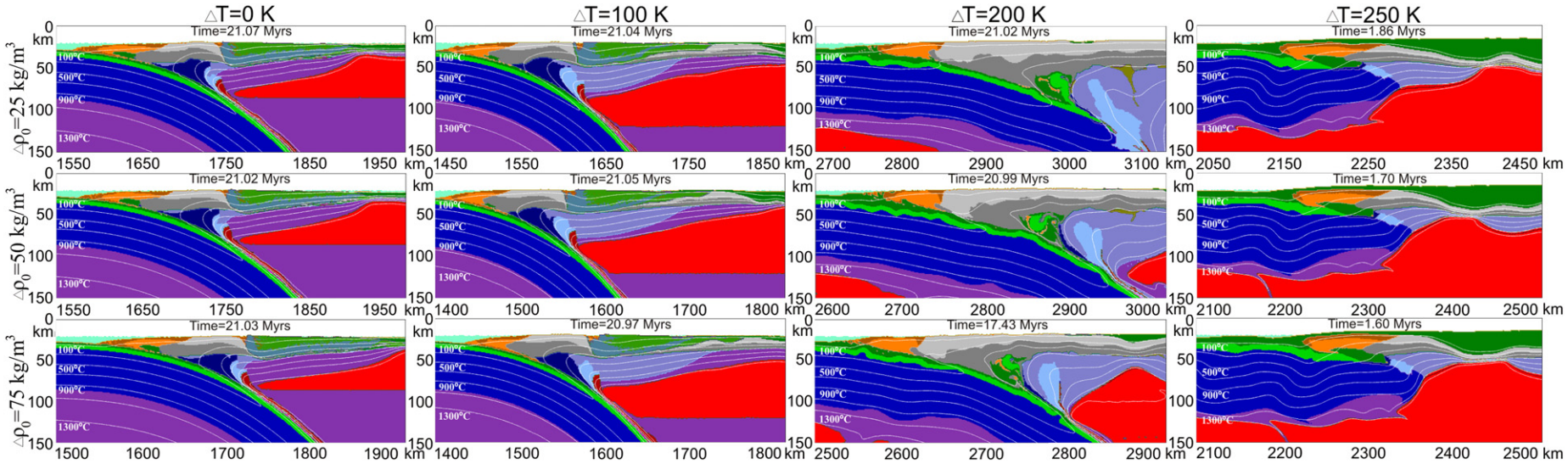

Fig. 11. Snapshots from numerical experiments in which the density contrast between the continental and the oceanic lithospheric mantle is varied for a constant oceanic lithospheric mantle density (ρ_0) of 3300 kg/m^3 ($\Delta\rho_0$: 25, 50 and 75 kg/m^3) as well as the upper-mantle temperature ($\Delta T = 0$–250 K) (see text for details). The light lilac color indicates lower density continental lithospheric mantle.

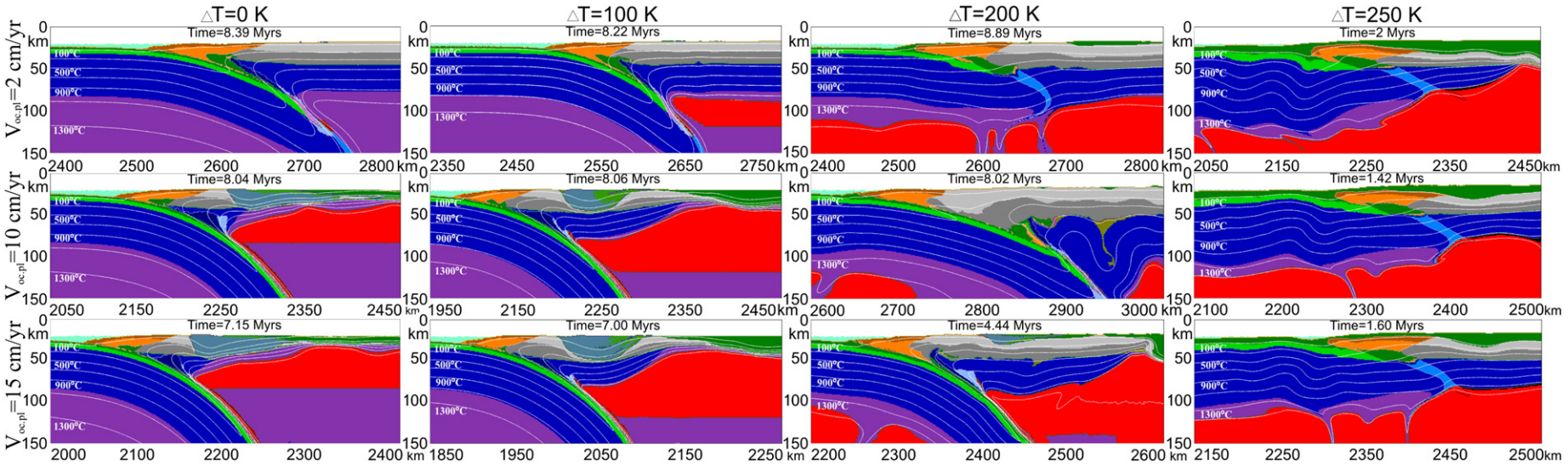

Fig. 12. Snapshots from numerical experiments with the variable velocity of the oceanic plate movement toward the continent (2, 10, 15 cm/yr) and upper-mantle temperature (ΔT: 0–250 K). At low velocity, three tectonic regimes are observed: the "modern subduction" regime ($\Delta T = 0$–200 K), the "pre-subduction" regime ($\Delta T = 200$–250 K) and the "no-subduction" regime (at $\Delta T = 250$ K) (see text for details).

"no-subduction" regime dominates (Fig. 9). Indeed, in the "pre-subduction" regime, underthrusting of a thicker oceanic plate proceeds at about one-third of the rate of the standard plate.

To investigate the high-temperature part of the "modern subduction" regime, we performed an additional experiment with a thickness of oceanic crust of 15 km at $\Delta T = 150$ K. In this experiment, the oceanic slab slowly sinks into the mantle, heats up to 700–900 °C and melts at depths of 50–130 km producing volcanic rocks in the arc area. The prescribed convergence of plates first results in buckling of the overriding plate that evolves into an asymmetric two-sided subduction (Fig. 9c) and finally into a one-sided oceanic–continental subduction.

It is well known that eclogitization of the oceanic crust may strongly increase its density which may partly compensate for any positive buoyancy effects of thicker oceanic crust. As shown by Ueda et al. (2008), even young and buoyant oceanic lithosphere may subduct spontaneously when conversion of basalt to eclogite is triggered by temporal dipping of the plate into the mantle. Therefore, we performed additional experiments for the "pre-subduction" regime at $\Delta T = 200$ K (Fig. 10) comparing cases with and without density changes related to phase transformations in the oceanic crust (including various dehydration reaction, particularly the conversion of basalt to eclogite). We used Gibbs free energy minimization (Connolly, 2005) for computing the density effects of gradual mertamorphic phase transformations in subducting oceanic crust (see Gerya et al., 2006 for methodology). Density effects of conversion of basalt to eclogite create significant negative slab buoyancy favoring a transition to self-sustaining subduction in the case of thicker oceanic crust. With standard present day thickness of the oceanic crust (7 km), the density effects of phase transformations are not strong enough to affect the underthrusting process, which still dominates model development (Fig. 10b). On the contrary, in the experiments with thicker oceanic crust (more than 10 km) subjected to conversion of basalt to eclogite the tectonic regime clearly changes from a "pre-subduction" type to the "modern subduction" type (Fig. 10d, f, h), and after about 7 Ma of underthrusting the eclogitized oceanic plate starts to sink forming one-sided subduction. However, in hotter experiments with $\Delta T = 250$ K corresponding to the "no-subduction" regime, when the thicker oceanic crust is subjected to phase transformations it does not lead to underthrusting (Fig. 10i, j).

3.4.2. Influence of density contrast between continental and oceanic lithospheric mantle

We also tested how the transition between the "modern subduction" regime and the "pre-subduction" regime is affected by a density contrast between the continental and the oceanic lithospheric mantle (Poudjom Djomani et al., 2001; Niu et al., 2003). A lowered standard density ($\Delta\rho_0 = 25$, 50 and 75 kg/m^3) was explored for 32 km thick continental mantle lithosphere (see the light lilac layer below the continent in Fig. 11). Experiments showed that at elevated (transitional) mantle temperature ($\Delta T = 200$ K) even a relatively low-density contrast of 25 kg/m^3 ($\rho_{0(\text{cont.})} = 3275$ kg/m^3) favors one-sided subduction starting after a prolonged period (ca. 20 Ma) of underthrusting and two-sided subduction. For higher density contrast of 50–75 kg/m^3, "modern subduction" starts even faster (after ca. 15 Ma). However, in hotter experiments ($\Delta T = 250$ K) originally corresponding to "no-subduction regime" (Fig. 3c) subduction does not occur and a chemical density contrast has no observable influence (Fig. 11).

3.4.3. Influence of oceanic plate velocity

All experiments described above were performed with a constant 5 cm/yr convergence velocity with the oceanic plate moving towards the continent. In order to test the influence of this parameter on the tectonic regime we varied the velocity from 2 to 15 cm/yr. The results confirm that transitions from the "modern subduction" regime to the "pre-subduction" and the "no-subduction" regimes with increasing mantle temperature are present at all oceanic plate velocities evaluated (Figs. 3 and 12). However, higher velocities broaden the stability of the "modern subduction" regime to higher mantle temperature (Fig. 12, $\Delta T = 200$ K).

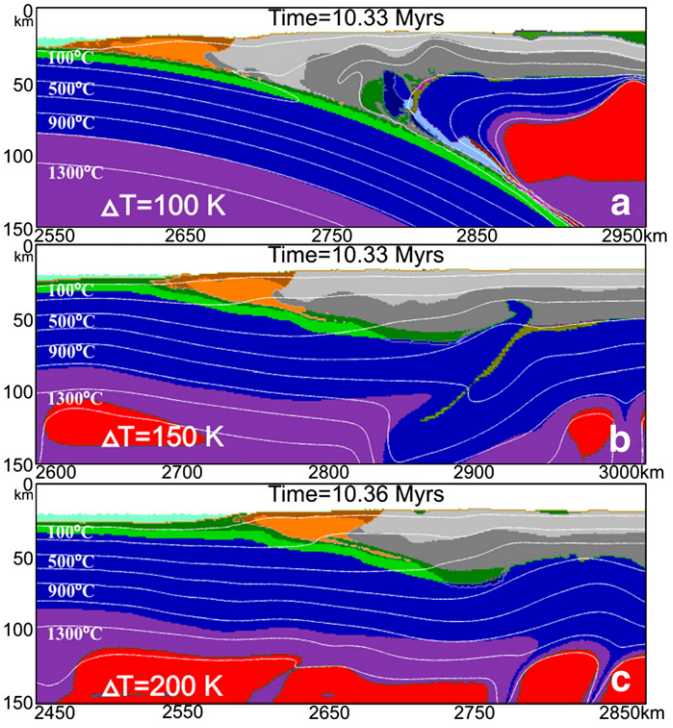

Fig. 13. Snapshots from numerical experiments without a prescribed weak fracture zone in the mantle between the oceanic and the continental plate at $\Delta T = 100$, 150 and 200 K. (a)—"modern subduction" regime, (b,c)—"pre-subduction" regime with underthrusting of the oceanic plate.

3.4.4. Influence of initial weak fracture zone presence

In all of the experiments subduction was initiated by prescribing a weak fracture zone in the mantle based on wet olivine rheology (Ranalli, 1995) and low plastic strength (internal friction coefficient of 0.1) between the oceanic and continental plate. To check the possible influence of this zone on the "pre-subduction" regime, a few additional experiments without this zone were also performed (Fig. 13). Fig. 13 shows that the tectonic style changes from the "modern subduction" regime to the "pre-subduction" regime without an initially prescribed weak zone being present, although intense underthrusting of the oceanic plates occurs at lower mantle temperature ($\Delta T = 150$ K) compared to the reference case (Fig. 3).

4. Discussion

In general, the results of our numerical experiments suggest changes in model behavior from the "modern subduction" regime to a "pre-subduction" regime and further to a "no-subduction" regime with increasing mantle temperature. Transitions between these regimes depend on a range of parameters (Fig. 14), but they are controlled primarily by the degree of weakening of plates by sub-lithospheric melts generated at elevated mantle temperatures such as those characteristic for the Precambrian.

4.1. Timing of initiation of plate tectonics and inhibiting factors

The link between geological observations and model results suggests that the transition to a plate tectonics regime with many features similar to modern Earth might have occurred during the Mesoarchean–Neoarchean time (ca. 3.2–2.5 Ga), which was suggested

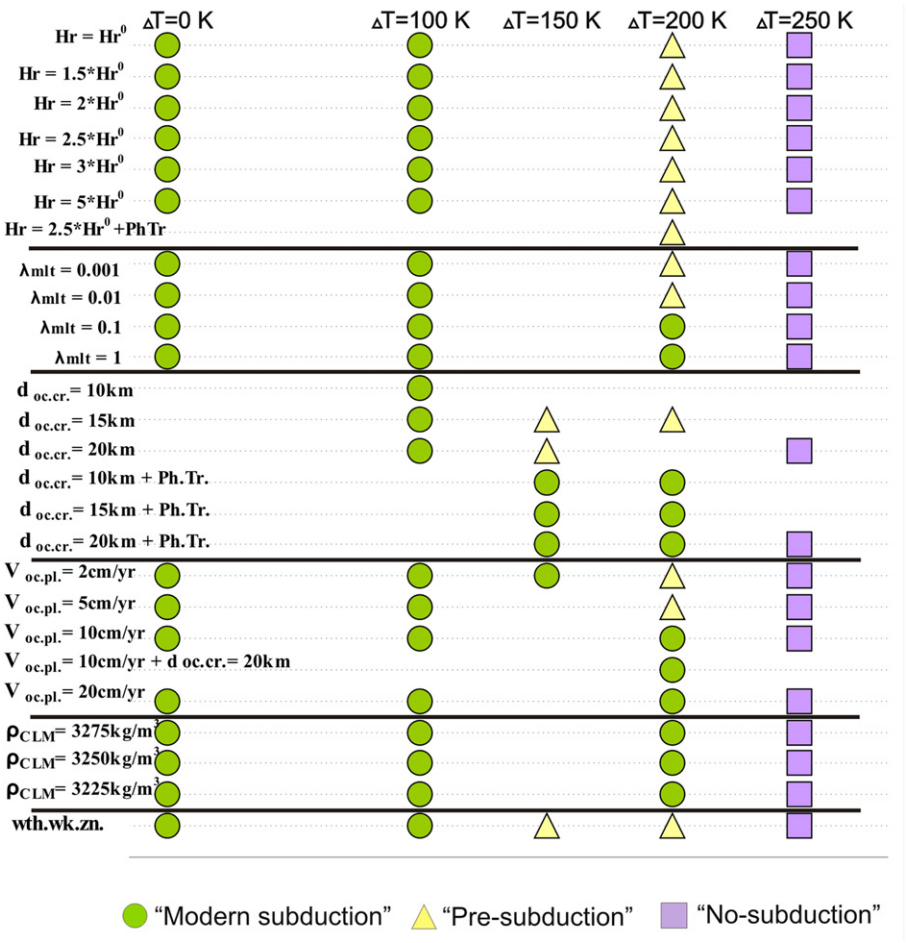

Fig. 14. Scheme of tectonic regimes observed versus the variables imposed in the numerical experiments (see text 3.4 for details). The experiments annotated with "+Ph.Tr." include the effects of phase transformations. λ_{melt}— melt weakening factor, $d_{oc.cr.}$—thickness of oceanic crust (with dependent variation of the lower crustal standard density of the lithospheric mantle), $V_{oc.pl}$—velocity of the oceanic plate, ρ_{CLM}—density of continental lithospheric mantle, wth.wk.zn.—experiments without a weak fracture zone in the mantle between the oceanic and the continental plates.

by Brown (2008) based on the occurrence of "paired metamorphic belts" since that time. In that case, the "pre-subduction" and the "no-subduction" regimes might correspond to the tectonic regimes during the Paleoarchean, Eoarchean and Hadean eras. Based on the model results, this transition might occur at an upper-mantle temperature about 160–175 K hotter than the present. That roughly correspond with the temperature at about 3 Ga (Abbott et al., 1994b; Labrosse and Jaupart, 2007; Sleep, 2007). In principal it is possible to determine the temperature of the ambient upper mantle by inverting the chemistry of the volcanic products of melting, which should allow us to determine the secular change in upper-mantle temperature. However, the genesis of volcanic rocks in the Archean, particularly komatiites, remains controversial, which means that the range of estimated temperatures for the upper mantle varies by several hundreds of degrees (Green, 1975; Arndt and Brooks, 1980; Stone et al., 1997; Arndt et al., 1998; de Wit, 1998; Wilson et al., 2003; Grove and Parman, 2004; Lee et al., 2009).

Rey and Coltice (2008) and Rey and Houseman (2006) point out that as the Moho temperature goes over 700 °C the strength of the upper mantle is significantly reduced to the point where the continental lithosphere is a bi-layer system consisting of strong upper crust above a weak crust and mantle ("crème brûlée-style" in Rey and Coltice (2008)). In these circumstances, the continental lithosphere is too weak to allow development of linear mountain belts and high plateaus. They showed that for most of the Archean the elevation of an orogenic plateau will be less than 2000 m, whereas the steady-state plateau elevation rapidly increases over geologic time since the Neoarchean. We observe the same results in our experiments (Fig. 4), with low elevations for the "pre-subduction" regime (less than 1500 m) and high elevations for the whole range of "modern subduction" regime parameters (up to 2500 m).

The transition from the Archean to the Proterozoic appears to record the major episodic change in tectonic regime in the Earth history (e.g. Taylor, 1987). Since that time, a subduction regime with the production of calc-alkaline volcanism has dominated tectonics on the Earth (Taylor, 1987). This change was not isochronous worldwide, but proceeded over an interval from about 3.1 Ga in southern Africa and Western Australia to about 2.5 Ga in parts of the Canadian Shield (Taylor and Mclennan, 1985, Chap. 8).

As discussed in the Introduction, many authors have suggested that the modern style of subduction and arc accretion processes may only have emerged towards the end of the Archean Eon (e.g. de Wit, 1998; Martin and Moyen, 2002; Griffin et al., 2003; Smithies et al., 2004; Martin et al., 2005; Brown, 2006, 2007, 2008; Condie and Pease, 2008). A form of plate tectonics may have operated earlier in the Hadean, Eoarchean and Paleoarchean (de Wit, 1998; Watson and Harrison, 2005; Hopkins et al., 2008), but subduction might have been very shallow and at low dips (e.g. Abbott et al., 1994a; de Wit, 1998; Smithies et al., 2003). In this case, it is argued that Archean "flat-subduction" did not form mantle wedge unlike modern subduction, although a mantle wedge contribution to the geochemistry of magmatic rocks has been recognized since the Mesoarchean (e.g. Smithies et al., 2005, 2007). Weak lithosphere in the Archean could favour distributed horizontal shortening with components of vertical

stretch (Cagnard et al., 2007). Cagnard et al. (2007) argue that horizontal shortening results in distributed thickening of crust and mantle ductile layers, which might inhibit subduction in the Archean (cf. Chardon et al., 2008, 2009).

Our results for the "pre-subduction" regime confirm these suggestions based on geological, geochemical and petrological arguments. During the "pre-subduction" regime we observe underthrusting without formation of a mantle wedge, consistent with the proposal of Archean "flat-subduction". Only after the transition to the "modern subduction" regime does the oceanic plate start to sink deep into the mantle to form a mantle wedge, which could contribute to forming magmatic rocks with a distinctive geochemistry.

On modern Earth, very low slab dips commonly are associated with the presence of unusually thick oceanic crust (up to 20–30 km) due to the presence of oceanic plateaus, aseismic ridges or seamount chains (McGeary et al., 1985; Gutscher et al., 2000a). As a consequence, many authors have suggested that a similar style of subduction characterized by very low slab dips might have been widespread in the Archean, based on the inference of thicker oceanic crust on a hotter Earth. However, very low slap dips also have been attributed to the active advance towards the trench of the overriding plate (van Hunen et al., 2002a, 2002b) and the presence of a low-pressure mantle wedge above the subducting slab causing it to rise (Tovish et al., 1978); van Hunen et al. (2004) have attributed very low slab dips to a combination of these mechanisms.

In some cases, very low slab dips may be due to the subduction of very young (<5 Ma), buoyant oceanic crust, which has been linked to the generation of adakites and, based on some similarities in geochemistry, the generation of Precambrian tonalite–trondhjemite–granodiorite suite magmas (Defant and Drummond, 1990; Drummond and Defant, 1990). In addition, flat subduction associated with the presence of unusually thick oceanic crust has been suggested as a mechanism to facilitate melting of older oceanic lithosphere (Gutscher et al., 2000b), which also has been invoked as a mechanism for the generation of Archean tonalite–trondhjemite–granite suite magmas (Smithies, 2000). Our results show that the main cause of very low slab dips, expressed as underthrusting in the experiments, is the weakening of the oceanic plate induced by the emplacement of sub-lithospheric melts into the lithosphere. The thickness of the oceanic crust is of minor importance since the weaker oceanic plants cannot produce normal one-sided subduction.

In experiments with an increased convergence velocity and the oceanic plate moving towards the continent, mimicking the postulated faster tempo of plate tectonics in the Archean (Davies, 1992), a broadening of the stability of the "modern subduction" regime to higher mantle temperatures is observed. However, the conclusions based on recent modeling of mantle evolution by Korenaga (2006) and an investigation of passive margins through Earth history by Bradley (2008) both suggest that plate tectonics might have been more sluggish in the Archean. If correct, this could contribute to dominance of the "pre-subduction" regime with underthrusting in the early Archean. Indeed, conclusions based on 2D numerical models still need to be tested with 3D approaches since the effects of the third dimension for plate dynamics and geometries can be quite significant (e.g. Tackley, 2000, 2008; Rey and Houseman, 2006).

The numerical models of Davies (2006) and van Hunen and van den Berg (2008) were designed to address the viability of plate tectonics on a hotter early Earth. Based on their experiments, compositional buoyancy resulting from thicker crust and harzburgite layers might be a serious limitation for initiation of subduction, and a different mode of downwelling (cf. Davies, 1992) or 'sub-lithospheric' subduction (van Hunen and van den Berg, 2008) might have characterized Earth in the Archean. van Hunen and van den Berg (2008) showed that eclogitization may significantly relax the limitation imposed by compositional buoyancy for a developed, ongoing subduction process, in which case the main factor inhibiting normal subduction might be slab breakoff.

Our experiments exploring the subduction process close to the surface and including melting show that the main limitation on the initiation of "modern subduction" is the presence of melt-bearing sub-lithospheric mantle and conversion of basalt to eclogite in the oceanic crust may help subduction if thicker oceanic crust ($\geq$10 km) is present.

Our experiments with ΔT~250 K show extremely weak plates that are strongly internally deformable and commonly fragmented by new spreading centers. Confirmation of these results suggesting plate fragmentation due to the weaker lithosphere may be found in the self-consistent generation of tectonic plates in the mantle convection simulations of Tackley (2000). Based on these self-consistent, time-dependent, three-dimensional models, Tackley (2000) determined that there is an increase in the number of plates with decreasing yield stress. At low yield stress he observed models characterized by many small plates with pronounced two-sided convergent boundaries but diffuse spreading centers. At higher yield stress, plate-like behavior was improved and the number of plates was reduced. A similar tendency is observed in our experiments for the transition from the "no-subduction" to the "pre-subduction" regime.

4.2. Formation of Archean TTG and adakites

Geochemical and petrological data from magmatic rocks have been used to identify tectonic processes during the Precambrian. Two of the voluminous rock groups preserved in the Precambrian crustal record in granite–greenstone belts are the tonalite–trondhjemite–granodiorite suite (TTG) and the adakite suite of intermediate-to-felsic volcanic rocks, respectively. The petrogenesis of these suites in the Precambrian is still debated (e.g. Martin and Moyen, 2002; Condie, 2005; Martin et al., 2005; Moyen, 2009). Arguments have been made that these suites could form in one or both of two different regimes: the first regime is connected with plume tectonics (e.g. Chambell and Hill, 1988; Zegers and Van Keken, 2001), which will not be discussed in detail here; and, the second regime is connected with a style of plate tectonics in which one plate moves under another (Smithies, 2000; Kamber et al., 2002; Condie, 2005), which is discussed below, where formation of these suites is thought to occur by partial melting of a sinking oceanic plate (e.g. Defant and Drummond, 1990; Gutscher et al., 2000b; Martin et al., 2005). This later assumption is quite consistent with our models.

According to Condie (2005), adakites might be formed by partial melting of sinking oceanic crust whereas TTGs most likely were formed by partial melting of the lower continental crust in arc systems or in the deep roots of oceanic plateaus (Willbold et al., 2009). This conclusion is in good agreement with our results for the "pre-subduction" regime, where both lower continental crust and sinking oceanic crust in the frontal area start to melt (Fig. 3b). These zones of partial melting may give rise to both TTGs and adakites. The conditions for formation of TTGs and adakites are quite similar, requiring T of 700–800 °C and a depth of 40–80 km, which is in good agreement with our results. Furthermore, it has been suggested that Archean adakites were formed without any interaction with a mantle wedge (e.g. de Wit, 1998; Smithies et al., 2003; Condie, 2005; Martin et al., 2005), which is also consistent with our models. In the case of underthrusting, oceanic lithosphere is thrust under the continental lithosphere without development of an intervening mantle wedge (Fig. 3b). A mantle wedge has contributed to magma genesis only since the Neoarchean, and even then it was not always involved (Martin, 1999; Martin et al., 2005; Smithies et al., 2005, 2007).

4.3. Formation of Archean UHT and E–HPG terranes

During the Mesoarchean–Neoarchean, 'paired metamorphic belts' appear for the first time in the geological record (Brown, 2006). The occurrence of both ultrahigh-temperature (UHT) and eclogite–high-pressure granulite (E–HPG) metamorphism—reflecting a duality of thermal regimes—might mark the onset of a "Proterozoic plate tectonics"

regime, which evolved during a Neoproterozoic transition to the modern plate tectonics regime, characterized by colder subduction as chronicled by HP–UHPG (high-pressure–ultrahigh-pressure) metamorphism.

UHT granulite metamorphism is dominantly a Neoarchean to Cambrian phenomenon, although it may be inferred at depth in some Phanerozoic orogens, whereas E–HPG metamorphism occurs from the Neoarchean to the Mesozoic, although in both cases occurrences during the Neoarchean-to-Paleoproterozoic transition are sporadic (Brown, 2007, 2008). In our numerical models, there are indeed areas which could correspond to conditions for UHT and E-HPG metamorphism in the "pre-subduction" regime. UHT granulites could form from the residue after separation of melts from the melt-bearing areas of the lower continental crust (Fig. 5). Temperatures in this area vary from 700 °C to more than 900 °C, which is the minimum temperature needed for the formation of UHT granulites, at depth of about 40 km; this zone is also a potential area for formation of a backarc basin in the "modern subduction" regime.

In addition, there are other mechanisms that potentially may lead to UHT granulite formation. For example, modest thickening of Archean continental crust with its higher radiogenic heat production, combined with thermal blanketing by the emplacement of continental flood basalts (e.g. Rey et al., 2003), might provide an alternative tectonic scenario for the generation of UHT granulite metamorphism in the Neoarchean.

E-HPG complexes could form by oceanic plate subduction up to depths of about 50 km at high temperature, where after an interval of time a segment of crust may separate from the plate and start to rise (Fig. 5 red marker). Metamorphic conditions for E-HPG metamorphism are 750–1000 °C at 1.5–2.5 GPa (Brown, 2007). The temperature in the transitional experiment for the ascending area is about 150 °C less than minimal one for E-HPG metamorphism. But, if we take into account previous underthrusting, the temperature in the frontal zone of the oceanic plate could exceed 700 °C. The frontal zone of the sinking oceanic plate is the part of the plate that may move upwards after the transition from the "pre-subduction" to the "modern subduction" regime when the slab became stronger and started to sink deep into the mantle. Our experimental results are consistent with the appearance of both UHT and EHPG complexes since the Mesoarchean–Neoarchean.

Unresolved is the question of the absence of ultrahigh-pressure (UHP) metamorphic complexes before the Neoproterozoic. As Vlaar and van den Berg (1991) assume, this may be a result of excess buoyancy of oceanic lithosphere preventing collapse into the underlying asthenosphere. They showed that absence of UHP metamorphic rocks prior to the late Precambrian may be related to a secular change in the rheological strength of subducting slabs. Our model results show the change in tectonic regimes with changing strength of the plates confirming this statement. Rheologically weaker plates are not able to sustain stresses arising from deep subduction of positively buoyant crustal rocks. This may in turn preclude formation of deeply penetrating crustal channels necessary for the formation and exhumation of UHP rocks (e.g. Gerya et al., 2008b; Warren et al., 2008b). The recent modeling of Warren et al. (2008a) with lower initial crustal strength shows detachment of the crust from the subducting slab at shallower depths than those necessary for formation of UHP metamorphic complexes and lower exhumation rates due to a reduced effective pressure gradient. Based on modeling by Burov and Yamato (2008), a strong mantle is a minimum requirement to force positively buoyant crust to greater depth.

4.4. Effects of imposed convergence condition

In our numerical models, the driving mechanisms of subduction are a combiniation of the forces of "plate push" (prescribed constant convergence velocity) and "slab pull" (temperature induced density contrast between the subducted lithosphere and surrounding mantle). This type of boundary condition is applied widely in numerical models of subduction and collision (e.g. Burg and Gerya, 2005; Warren et al., 2008b; Currie et al., 2007), assuming that in a globally confined system of plates, "external push" imposed on a plate (and coming from different slabs) can be significant. Spontaneously growing slab pull in this type of model mainly regulates slab bending dynamics and slab retreat velocity (e.g. Gorczyk et al., 2007). Whereas this approach is widely accepted for modern style subduction it becomes less appropriate for Precambrian processes when oceanic plates may lose coherency due to weakening induced by emplacement of sub-lithospheric melts into the lithosphere, as identified in this study. Therefore, model predictions for the actual geometry and dynamics in the "pre-subduction" and "no subduction" regimes should be considered with caution, and further studies of these regimes exploring more consistent forcing-free boundary conditions (e.g. Tackley, 2000; Gerya et al., 2008b; Nikolaeva et al., 2008) are needed in the future.

5. Conclusions

Based on a 2D petrological–thermomechanical numerical model of oceanic subduction we systematically investigated the dependence of tectono-metamorphic and magmatic regimes at an active margin on upper-mantle temperature, crustal radiogenic heat production, lithospheric weakening by fluids and melts, variable thickness of oceanic crust, difference in densities of continental and oceanic lithospheric mantle, prescribed velocity of the oceanic plate toward the continent, and phase transformations. Experiments revealed the first-order changes from the modern style of subduction through a transitional "pre-subduction" regime to a "no-subduction" regime with increasing upper-mantle temperature. These transitions take place at upper-mantle temperatures elevated by around 160–175 K and 200–250 K above the present-day values, respectively. Based on geological observations and model results we can refer the first transition to the modern plate tectonics regime to the Mesoarchean–Neoarchean (2.5–3.2 Ga). A crucial difference between the "modern subduction" style and the tectonic regime at high mantle temperatures is the presence of continuously produced sub-lithospheric melts that weaken the overlaying lithosphere. As a consequence plates become very weak, lose coherency and do not produce self-sustaining one-sided subduction. The "pre-subduction" regime is very sensitive to most of the parameters explored in our modeling, which correlates well with the variation in signatures recognized in the Archean geological record.

Acknowledgments

This work was supported by ETH Research Grants TH-12/05-3, TH-0807-3, SNF Research Grant 200021-113672/1, 200021-116381/1, the RF President Program "Leading Scientific School of Russia" (Grant #1949.2008.5) to TVG.

References

Abbott, D., Drury, R., Smith, W.H., 1994a. Flat to steep transition in subduction style. Geology 22 (10), 937–940.
Abbott, D., Burgess, L., Longhi, J., Smith, W.H.F., 1994b. An empirical thermal history of the Earth's upper mantle. Journal of Geophysical Research 99, 13835–13850.
Arndt, N., Brooks, C., 1980. Komatiites. Geology 8, 155–156.
Arndt, N., Ginibre, C., Chauvel, C., Albarede, F., Cheadle, M., Herzberg, C., Jenner, G., Lahaye, Y., 1998. Were komatiites wet? Geology 26, 739–742.
Benn, K., Mareschal, J.-C., Condie, K., 2005. Archean Geodynamics and Environments: Geophysical Union, Geophysical Monograph Series, vol. 64. 320 pp.
Bittner, D., Schmeling, H., 1995. Numerical modeling of melting processes and induced diapirism in the lower crust. Geophysical Journal International 123, 59–70.
Bradley, D.C., 2008. Passive margins through earth history. Earth-Science Reviews 91, 1–26.
Brown, M., 2006. Duality of thermal regimes is the distinctive characteristic of plate tectonics since the Neoarchean. Geology 34 (11), 961–964.
Brown, M., 2007. Metamorphic conditions in orogenic belts: a record of secular change. International Geology Review 49 (3), 193–234.

Brown, M., 2008. Characteristic thermal regimes of plate tectonics and their metamorphic imprint throughout Earth history. In: Condie, K.C., Pease, V. (Eds.), When did Earth First Adopt a Plate Tectonics Mode of Behavior? The Geological Society of America, Special paper, vol. 440, pp. 97–128.
Burg, J.-P., Gerya, T.V., 2005. The role of viscous heating in Barrovian metamorphism of collisional orogens: thermomechanical models and application to the Lepontine Dome in the Central Alps. Journal of Metamorphic Geology 23, 75–95.
Burov, E.B., Watts, A.B., 2006. The long-term strength of continental lithosphere: "jelly sandwich" or "creme brulee"? GSA Today 16, 4–10.
Burov, E., Yamato, P., 2008. Continental plate collision, P–T–t–z conditions and unstable vs. stable plate dynamics: insights from thermo–mechanical modeling. Lithos 103, 178–204.
Cagnard, F., Brun, J.-P., Gapais, D., 2007. Modes of thickening of analogue weak lithospheres. Tectonophysics 421, 145–160.
Carlson, R.L., Miller, D.J., 2003. Mantle wedge water contents estimated from seismic velocities in partially serpentinized peridotites. Geophysical Research Letters 30 (5).
Chambell, I.H., Hill, R.I., 1988. A two-stage model for the formation of the granite–greentsone terrains of the Kalgoorlie–Norseman area, Weatern Australia. Earth and Planetary Science Letters 90, 11–25.
Chardon, D., Jayananda, M., Chetty, T.R.K., Peucat, J.-J., 2008. Precambrian continental strain and shear zone patterns: South Indian case. Journal of Geophysical Research–Solid Earth 113 (B8), B08402.
Chardon, D., Gapais, D., Cagnard, F., 2009. Flow of ultra-hot orogens: a view from the Precambrian, clues for the Phanerozoic. Tectonophysics 477, 105–118.
Christensen, N.I., Yuen, D.A., 1985. Layered convection induced by phase-transitions. Journal of Geophysical Research-Solid Earth and Planets 90, 291–300.
Clauser, C., Huenges, E., 1995. Thermal conductivity of rocks and minerals. In: Ahrens, T.J. (Ed.), Rock Physics and Phase Relations: AGU Reference Shelf, vol. 3, pp. 105–126.
Condie, K.C., 2005. TTGs and adakites: are they both slab melts? Lithos 80 (1–4), 33–44.
Condie, K.C., Pease, V., 2008. When did Plate Tectonics Begin on Planet Earth? In: The Geological Society of America, Special Paper, vol. 440. 294 pp.
Connolly, J.A.D., 2005. Computation of phase equilibria by linear programming: a tool for geodynamic modeling and its application to subduction zone decarbonation. Earth and Planetary Science Letters 236, 524–541.
Currie, C.A., Beaumont, C., Huismans, R.S., 2007. The fate of subducted sediments: a case for backarc intrusion and underplating. Geology 35 (12), 1111–1114.
Davies, G.F., 1992. On the emergence of plate-tectonics. Geology 20 (11), 963–966.
Davies, G.F., 1999. The role of hydraulic fractures in generating intermediate depth earthquakes and subduction zone magmatism. Nature 398, 142–145.
Davies, G.F., 2006. Gravitational depletion of the early Earth's upper mantle and the viability of early plate tectonics. Earth and Planetary Science Letters 243 (3–4), 376–382.
Defant, M.J., Drummond, M.S., 1990. Derivation of some modern arc magmas by melting of young subducted lithosphere. Nature 347, 662–665.
de Wit, M.J., 1998. On Archean granites, greenstones, cratons and tectonics: does the evidence demand a verdict? Precambrian Research 91 (1–2), 181–226.
Drummond, M.S., Defant, M.J., 1990. A model for trondhjemite–tonalite–dacite genesis and crustal growth via slab melting—Archean to modern comparisons. Journal of Geophysical Research–Solid Earth and Planets 95, 21503–21521.
Elliott, T., Plank, T., Zindler, A., Wjite, W., Bourdon, B., 1997. Element transport from slab to volcanic front at the Mariana arc. Journal of Geophysical Research 102, 14991–15019.
Flament, N., Coltice, N., Rey, P.F., 2008. A case for late-Archean continental emergence from thermal evolution models and hypsometry. Earth and Planetary Science Letters 275, 3–4.
Gerya, T.V., Yuen, D.A., 2003a. Rayleigh-Taylor instabilities from hydration and melting propel "cold plumes" at subduction zones. Earth and Planet Science Letters 212, 47–62.
Gerya, T.V., Yuen, D.A., 2003b. Characteristics-based marker-in-cell method with conservative finite-differences schemes for modeling geological flows with strongly variable transport properties. Physics of the Earth and Planetary Interiors 140, 295–318.
Gerya, T.V., Yuen, D.A., 2007. Robust characteristics method for modelling multiphase visco-elasto-plastic thermo–mechanical problems. Physics of the Earth and Planetary Interiors 163, 83–105.
Gerya, T.V., Connolly, A.D., Yuen, D.A., Gorczyk, W., Capel, A.M., 2006. Seismic implications of mantle wedge plumes. Physics of the Earth and Planetary Interiors 156, 59–74.
Gerya, T.V., Connolly, J.A.D., Yuen, D.A., 2008a. Why is terrestrial subduction one-sided? Geology 36 (1), 43–46.
Gerya, T.V., Perchuk, L.L., Burg, J.-P., 2008b. Transient hot channels: perpetrating and regurgitating ultrahigh-pressure, high-temperature crust-mantle associations in collision belts. Lithos 103, 236–256.
Gorczyk, W., Willner, A.P., Connolly, J.A.D., Burg, J.-P., 2007. Physical controls of magmatic productivity at Pacific-type convergent margins: new insights from numerical modeling. Physics of the Earth and Planetary Interiors 163 (1–4), 209–232.
Green, D.H., 1975. Genesis of Archean periodotitic magmas and constraints on Archean geothermal gradients and tectonics. Geology 3, 15–18.
Griffin, W.L., O'Reilly, S.Y., Abe, N., Aulbach, S., Davies, R.M., Pearson, N.J., Doyle, B.J., Kivi, K., 2003. The origin and evolution of Archean lithospheric mantle. Precambrian Research 127 (1–3), 19–41.
Grove, T.L., Parman, S.W., 2004. Thermal evolution of the Earth as recorded by komatiites. Earth and Planetary Science Letters 219, 173–187.
Grove, T.L., Chatterjee, N., Parman, S.W., Medard, E., 2006. The influence of H_2O on mantle wedge melting. Earth and Planetary Science Letters 249, 74–89.
Gutscher, M.A., Maury, R., Eissen, J.P., Bourdon, E., 2000a. Can slab melting be caused by flat subduction? Geology 28, 535–538.
Gutscher, M.A., Spakman, W., Bijwaard, H., Engdahl, E.R., 2000b. Geodynamics of flat subduction: seismicity and tomographic constraints from the Archean margin. Tectonics 19, 814–833.
Hamilton, W.B., 1998. Archean magmatism and deformation were not products of plate tectonics. Precambrian Research 91 (1–2), 143–179.
Hawkesworth, C.J., Turner, S.P., McDermott, F., Peate, D.W., van Calsteren, P., 1997. U–Th isotopes in arc magmas: implications for element transfer from the subducted crust. Science 276, 551–555.
Holtzman, B.K., Kohlstedt, D.L., 2007. Stress-driven melt segregation and strain partitioning in partially molten rocks: effects of stress and strain. Journal of Petrology 48, 2379–2406.
Hopkins, M., Harrison, T.M., Manning, C.E., 2008. Low heat flow inferred from >4 Gyr zircons suggests Hadean plate boundary interactions. Nature 456, 493–496.
Johannes, W., 1985. The significance of experimental studies for the formation of migmatites. In: Ashworth, V.A. (Ed.), Migmatites, Blackie, Glasgow, pp. 36–85.
Kamber, B.S., Ewart, A., Collerson, K.D., Bruce, M.C., McDonald, G.D., 2002. Fluid-mobile trace element constraints on the role of slab melting and implications for Archaean crustal growth models. Contributions to Mineralogy and Petrology 144, 38–56.
Kohlstedt, D.L., Zimmerman, M.E., 1996. Rheology of partially molten mantle rocks. Annual Review of Earth and Planetary Sciences 24, 41–62.
Korenaga, J., 2006. Archean geodynamics and thermal evolution of Eath. Archean Geodynamics and Environments. AGU Geophysical Monograph Series 164, 7–32.
Labrosse, S., Jaupart, C., 2007. Thermal evolution of the Earth: secular changes and fluctuations of plate characteristics. Earth and Planetary Science Letters 260, 465–481.
Lee, C.-T.A., Luffi, P., Plank, T., Dalton, H., Leeman, W.P., 2009. Constraints on the depths and temperatures of basaltic magma generation on Earth and other terrestrial planets using new thermobarometers for mafic magmas. Earth and Planetary Science Letters 279, 20–33.
Martin, H., 1999. Adakitic magmas: modern analogues of Archaean granitoids. Lithos 46, 411–429.
Martin, H., Moyen, J.-F., 2002. Secular changes in tonalite–trondhjemite–granodiorite composition as markers of the progressive cooling of Earth. Geology 30 (4), 319–322.
Martin, H., Smithies, R.H., Rapp, R., Moyen, J.F., Champion, D., 2005. An overview of adakite, tonalite–trondhjemite–granodiorite (TTG), and sanukitoid: relationships and some implications for crustal evolution. Lithos 79, 1–24.
McGeary, S., Nur, A., Benavraham, Z., 1985. Spatial gaps in arc volcanism—the effect of collision or subduction of oceanic plateaus. Tectonophysics 119, 195–221.
Moresi, L., Solomatov, V.S., 1998. Mantle convection with a brittle lithosphere: thoughts on the global tectonic styles of the Earth and Venus. Geophysical Journal International 133, 669–682.
Moyen, J.-F., 2009. High Sr/Y and La/Yb ratios: the meaning of the "adakitic signature". Lithos 112, 556–574.
Nikolaeva, K., Gerya, T.V., Connolly, J.A.D., 2008. Numerical modelling of crustal growth in intraoceanic volcanic arcs. Physics of the Earth and Planetary Interiors 171 (1–4), 336–356.
Niu, Y., O'Hara, M.J., Pearce, J.A., 2003. Initiation of subduction zones as a consequence of lateral compositional buoyancy contrast within the lithosphere: a petrological perspective. Journal of Petrology 44, 851–866.
O'Neil, C., Lenardic, A., Moresi, L., Torsvik, T.H., Lee, C.-T.A., 2007a. Episodic Precambrian subduction. Earth and Planetary Science Letters 262, 552–562.
O'Neil, C., Jellinek, A.M., Lenardic, A., 2007b. Conditions for the onset of plate tectonics on terrestrial planets and moons. Earth and Planetary Science Letters 261, 20–32.
Pearce, J.A., 2008. Geochemical fingerprinting of oceanic basalts with applications to ophiolite classification and the search for Archean oceanic crust. Lithos 100, 14–48.
Poli, S., Schmidt, M.W., 2002. Petrology of subducted slabs,. Annual Review of Earth and Planetary Sciences 30, 207–235.
Poudjom Djomani, Y.H., O'Reilly, S.Y., Griffin, W.L., Morgan, P., 2001. The density structure of subcontinental lithosphere through time. Earth and Planet Science Letters 184, 605–621.
Ranalli, G., 1995. Rheology of the Earth. InChapman and Hall, London, p. 413.
Regenauer-Lieb, K., Yuen, D.A., Branlund, J., 2001. The initiation of subduction: criticality by addition of water? Science 294, 578–580.
Rey, P.F., Coltice, N., 2008. Neoarchean lithospheric strengthening and the Earth's geochemical reservoirs. Geology 36 (8), 635–638.
Rey, P., Houseman, G., 2006. Lithospheric scale gravitational flow: the impact of body forces on orogenic processes from Archaean to Phanerozoic. In: Buiter, S.J.H., Schreurs, G. (Eds.), Analogue and Numerical Modelling of Crustal-scale Processes: Geological Society of London Special Publication, vol. 253, pp. 153–167.
Rey, P.F., Philippot, P., Thébaud, N., 2003. Contribution of mantle plumes, crustal thickening and greenstone blanketing to the 2.75–2.65 Ga global crisis. Precambrian Research 127, 43–60.
Rosenberg, C.L., Handy, M.R., 2005. Experimental deformation of partially melted granite revisited: implications for the continental crust. Journal of Metamorphic Geology 23, 19–28.
Schmeling, H., Babeyko, A.Y., Enns, A., Faccenna, C., Funiciello, F., Gerya, T., Golabek, G.J., Grigull, S., Kaus, B.J.P., Morra, G., Schmalholz, S.M., van Hunen, J., 2008. Benchmark comparison of spontaneous subduction models—towards a free surface. Physics of the Earth and Planetary Interiors 171 (1–4), 198–223.
Schmidt, M., Poli, S., 1998. Experimentally based water budgets for dehydrating slabs and consequences for arc magma generation. Earth and Planetary Letters 163, 361–379.
Sleep, N.H., 2007. Plate tectonics through time. In: Stevenson, D. (Ed.), Treatise on Geophysics: Evolution of the Earth, vol. 9, pp. 145–169.
Smithies, R.H., 2000. The Archaean tonalite–trondhjemite–granodiorite (TTG) series is not an analogue of Cenozoic adakite. Earth and Planetary Science Letters 182, 115–125.

Smithies, R.H., Champion, D.C., Cassidy, K.F., 2003. Formation of Earth's early Archaean continental crust. Precambrian Research 127 (1–3), 89–101.
Smithies, R.H., Champion, D.C., Sun, S.S., 2004. The case for Archaean boninites. Contributions to Mineralogy and Petrology 147, 705–721.
Smithies, R.H., Champion, D.C., Van Kranendonk, M.J., Howard, H.M., Hickman, A.H., 2005. Modem-style subduction processes in the Mesoarchaean: geochemical evidence from the 3.12 Ga Whundo intra-oceanic arc. Earth and Planetary Science Letters 231, 221–237.
Smithies, R.H., Van Kranendonk, M.J., Kranendonk, M.J., Champion, D.C., 2007. The Mesoarchean emergence of modern-style subduction. Gondwana Research 11, 50–68.
Stern, R.J., 2005. Evidence from ophiolites, blueschists, and ultrahigh-pressure metamorphic terranes that the modern episode of subduction tectonics began in Neoproterozoic time. Geology 33, 557–560.
Stern, R.J., 2007. When and how did plate tectonics begin? Theoretical and empirical considerations. Chinese Science Bulletin 52 (5), 578–591.
Stone, W.E., Deloule, E., Larson, M.S., Lesher, C.M., 1997. Evidence for hydrous high-MgO melts in the Precambrian. Geology 25, 143–146.
Tackley, P., 2000. Self-consistent generation of tectonic plates in time-dependent, three-dimensional mantle convection simulations. 1. Pseudoplastic yielding. Geochemistry, Geophysics, Geosystems 1.
Tackley, P.J., 2008. Modelling compressible mantle convection with large viscosity contrasts in a three-dimensional spherical shell using the yin-yang grid. Physics of the Earth and Planetary Interiors 171, 7–18.
Taylor, S.R., 1987. Geochemical and petrological significance of the Archaean–Proterozoic boundary. Geological Society, London, Special Publications 33, 3–8.
Taylor, S.R., Mclennan, S.M., 1985. The Continental Crust: its Composition and Evolution. Blackwell Scientific Publications, Oxford.
Toth, J., Gurnis, M., 1998. Dynamics of subduction initiation at preexisting fault zones. Journal of Geophysical Research-Solid Earth 103, 18053–18067.
Tovish, A., Schubert, G., Luyendyk, B.P., 1978. Mantle flow pressure and the angle of subduction—non-Newtonian corner flows. Journal of Geophysical Research 83, 5892–5898.
Turcotte, D.L., Schubert, G., 2002. Geodynamics. InCambridge University Press, p. 456.
Ueda, K., Gerya, T., Sobolev, S.V., 2008. Subduction initiation by thermal–chemical plumes: numerical studies. Physics of the Earth and Planetary Interiors 171, 296–312.
van Hunen, J., van den Berg, A.P., Vlaar, N.J., 2002a. The impact of the South-American plate motion and the Nazca Ridge subduction on the flat subduction below South Peru. Geophysical Research Letters 29 (14), 1690.
van Hunen, J., van den Berg, A.P., Vlaar, N.J., 2002b. On the role of subducting oceanic plateaus in the development of shallow flat subduction. Tectonophysics 352, 317–333.
van Hunen, J., van den Berg, A.P., Blaar, N.J., 2004. Various mechanisms to induce present-day shallow flat subduction and implications for the younger Earth: a numerical parameter study. Physics of the Earth and Planetary Interiors 146, 179–194.
van Hunen, J., van den Berg, A., 2008. Plate tectonics on the early Earth: limitations imposed by strength and buoyancy of subducted lithosphere. Lithos 103, 217–235.
Vlaar, N.J., van den Berg, A.P., 1991. Continental evolution and archeaosealevels. In: Sabadini, R., Lambeck, K., Boschi, E. (Eds.), Glacial Isostasy, Sea-Level and Mantle Rheology. Kluwer.
Warren, C.J., Beaumont, C., Jamieson, R.A., 2008a. Deep subduction and rapid exhumation: role of crustal strength and strain weakening in continental subduction and ultrahigh-pressure rock exhumation. Tectonics 27, TC6002.
Warren, C.J., Beaumont, C., Jamieson, R.A., 2008b. Formation and exhumation of ultra-high pressure rocks during continental collision: role of detachment in the subduction channel. Geochemistry Geophysics Geosystems 9, Q04019.
Watson, E.B., Harrison, T.M., 2005. Zircon thermometer reveals minimum melting conditions on earliest Earth. Science 308, 841–844.
Willbold, M., Hegner, E., Stracke, A., Rocholl, A., 2009. Continental geochemical signatures in dacites from Iceland and implications for models of early Archaean crust formation. Earth and Planetary Science Letters 279, 44–52.
Wilson, A.H., Shirey, S.B., Carlson, R.W., 2003. Archaean ultra-depleted komatiites formed by hydrous melting of cratonic mantle. Nature 423, 858–861.
Zegers, T.E., Van Keken, P.E., 2001. Middle Archean continent formation by crustal delamination. Geology 29, 1083–1086.